

# Blind denoising diffusion models and the blessings of dimensionality

Zahra Kadkhodaie<sup>1,\*</sup>, Aram-Alexandre Pooladian<sup>2,\*</sup>  
 Sinho Chewi<sup>3</sup>, and Eero P. Simoncelli<sup>1,4</sup>

<sup>1</sup>Flatiron Institute, Simons Foundation.

<sup>2</sup>Foundations of Data Science, Yale University.

<sup>3</sup>Department of Statistics and Data Science, Yale University.

<sup>4</sup>Ctr. for Neural Science & Courant Institute, New York University.

[zkadkhodaie@flatironinstitute.org](mailto:zkadkhodaie@flatironinstitute.org)

[{aram-alexandre.pooladian,sinho.chewi}@yale.edu](mailto:{aram-alexandre.pooladian,sinho.chewi}@yale.edu)

[esimoncelli@flatironinstitute.org](mailto:esimoncelli@flatironinstitute.org)

February 11, 2026

## Abstract

We analyze, theoretically and empirically, the performance of generative diffusion models based on *blind denoisers*, in which the denoiser is not given the noise amplitude in either the training or sampling processes. Assuming that the data distribution has low intrinsic dimensionality, we prove that blind denoising diffusion models (BDDMs), despite not having access to the noise amplitude, *automatically* track a particular *implicit* noise schedule along the reverse process. Our analysis shows that BDDMs can accurately sample from the data distribution in polynomially many steps as a function of the intrinsic dimension. Empirical results corroborate these mathematical findings on both synthetic and image data, demonstrating that the noise variance is accurately estimated from the noisy image. Remarkably, we observe that schedule-free BDDMs produce samples of higher quality compared to their non-blind counterparts. We provide evidence that this performance gain arises because BDDMs correct the mismatch between the true residual noise (of the image) and the noise assumed by the schedule used in non-blind diffusion models.

## 1 Introduction

Diffusion models have emerged as the dominant methodology for generative modeling and solving inverse problems. In contrast to previous machine learning methods, such

---

\*Equal contribution.

as generative adversarial networks (Arjovsky et al., 2017), normalizing flows (Grathwohl et al., 2019), or variational autoencoders (Kingma and Welling, 2013), diffusion models are based on corresponding noise corruption and denoising processes (Sohl-Dickstein et al., 2015; Ho et al., 2020; Song et al., 2021b). In brief, sampling is achieved through discretizations of stochastic differential equations (SDEs) of the form

$$dX_t = \hat{b}_\theta(X_t, \sigma_t) dt + \sqrt{2a_t} dB_t, \quad (1)$$

where  $\hat{b}_\theta : \mathbb{R}^d \times \mathbb{R}_+ \rightarrow \mathbb{R}^d$  is an optimal denoiser,  $dB_t$  is standard Brownian motion, and  $(a_t)_{t \geq 0}$  are diffusion coefficients. The correctness of (1) as a method for sampling from the data distribution holds by design in continuous time, due to the nature of forward and backward diffusion processes (Föllmer, 1985) and the fact that an optimal denoiser computes a scaled version of the score function of the noisy data distribution (Miyasawa, 1961; Efron, 2011; Raphan and Simoncelli, 2011).

In practice, the denoiser is usually implemented as a parametric neural network that takes as input the noisy image (first argument,  $X_\sigma$ ) and the corresponding noise level (second argument,  $\sigma$ ), and is trained to denoise the noisy image. During sampling, (1) is discretized, and a noise schedule is prescribed to provide noise level arguments that ensure that the network follows the appropriate trajectory. Thus, the success of such generative algorithms hinge on training a high-quality denoiser and a noise schedule that allows  $\hat{b}_\theta$  to successfully denoise along the process.

What if the noise level is not passed to the network during training? The resulting *blind denoiser*, denoted  $\hat{s}_\theta : \mathbb{R}^d \rightarrow \mathbb{R}^d$  (see Section 2.2), must then effectively determine the noise level from the noisy image. Remarkably, blind denoising diffusion models (BDDMs) can be highly effective in sampling from complex distributions and in solving inverse problems (Kadkhodaie and Simoncelli, 2020, 2021). Sampling via BDDMs is based on discretizations of the following dynamics

$$dY_t = \hat{s}_\theta(Y_t) dt + \sqrt{2a_t} dB_t. \quad (2)$$

We emphasize that the drift term (i.e. first term) in (2) is *independent of time*, suggesting that these dynamics are closer to standard Langevin-type dynamics. But unlike (1), the convergence of this scheme is not clear from the outset. These observations lead us to our first motivating question:

*Is there a principled explanation for the empirical success of BDDMs?*

Beyond theoretical justification, we want to better understand the practical implications of blind denoisers for generative modeling. Indeed, BDDMs have “less information” (namely, they are not given the noise level) than their non-blind counterparts during both training and sampling. Moreover, prior work suggests that noise schedules and time embeddings are not required, minimizing the number of hyperparameters that must be tuned (Sun et al., 2025). Thus, we also ask:

*What are the computational advantages of BDDMs?*

## Contributions

This work provides the first mathematical justification for the success of blind denoising diffusion models.

**Blessings of dimensionality.** Motivated by empirical evidence (Olshausen and Field, 1996; Roweis and Saul, 2000; Chandler and Field, 2007; Hénaff et al., 2014; Pope et al., 2021; Brown et al., 2023), we identify **low intrinsic dimensionality** of the data distribution  $p_X$  as a natural condition that explains the success of BDDMs. Under this condition, we show that **BDDMs provably generate correct samples**. Specifically, as a corollary to our main results, we show that the distribution arising from (2), denoted  $p_{\text{alg}}$ , is close to  $p_X$  if the intrinsic dimension  $k$  is sufficiently small, i.e.,

$$D(p_X, p_{\text{alg}}) \leq \varepsilon \quad \text{if} \quad \frac{k^4}{\varepsilon^4} \ll d, \quad (3)$$

where  $D(\cdot, \cdot)$  corresponds to a “perceptual” metric between distributions (Corollary 3.10). Building on state-of-the-art works on low-dimensional adaptivity of diffusion models (Huang et al., 2024; Li and Yan, 2024; Potapchik et al., 2024; Liang et al., 2025; Tang and Yan, 2025), we then proceed to show that the **iteration complexity of BDDMs scales as  $k^2/\varepsilon^2$** .

Our theory also has predictive power: it identifies **canonical choices for the diffusion schedule  $(a_t)_{t \geq 0}$ , the prior over noise levels during training, and the step size schedule**. In particular, our theory suggests that **a constant stepsize suffices** for sampling, reducing the need to tune noise schedules. In fact, we show that BDDMs track an *implicit* noise schedule, whereby the law of  $Y_t$  in (2) approximates  $p_X * \mathcal{N}(0, \sigma_t^2 I)$  for a noise schedule given by

$$\sigma_t^2 = \sigma_0^2 e^{-2t} + 2 \int_0^t a_s e^{-2(t-s)} ds. \quad (4)$$

Key to our approach is the formal introduction of Bayesian statistical estimation of the noise level from a single noisy sample. In some cases, this problem is not solvable (e.g., if  $p_X$  is Gaussian distributed). However, we show that **low intrinsic dimensionality enables consistent estimation**. Both of these predictions—namely, that (i) BDDMs track the noise schedule (4) and (ii) the noise level is accurately learned in low intrinsic dimension—are confirmed by our experiments.

**Computational benefits of blind denoising.** Turning to our second main question, we compare the performance of blind and non-blind denoising diffusion models. Starting from the same initial noise sample and injecting the same noise along the trajectory, we find that the two diffusion models arrive at dramatically different sample images. We conjecture and verify experimentally that this deviation arises from a subtle but important empirical error in the non-blind setting: **along a discretized trajectory in the backward process, the noise prescribed by the explicit schedule and the true noise level on the noisy sample (i.e.,  $(x_\sigma, \sigma) \mapsto \hat{b}_\theta(x_\sigma, \sigma)$ ) do not match**. In contrast, BDDMs only operate on the noisy image as input, and follow an implicit noise schedule naturally inferred from the noisy image, and thus they do not face this mismatch. As a result, we observe that **BDDMs produce samples of both higher quality** in the constant step size regime.

## Related work

### Blind denoising (diffusion models)

BDDMs were introduced by Kadkhodaie and Simoncelli (2020, 2021), in which a blind deep neural network denoiser (Zhang et al., 2017) was used to sample from  $p_X$  in dynamics described in (2). Their capabilities for sampling and solving linear inverse problems were demonstrated empirically and their generalization (with respect to training set size) was examined by Kadkhodaie et al. (2024).

Several recent publications (e.g., Li and He, 2025; Wang and Du, 2025) train neural networks to learn dynamics without time inputs. Sun et al. (2025) show that noise conditioning is not required for sampling, and verify this empirically on dynamics which rely on explicit schedules. They also make partial initial progress on a theory for blind denoisers for diffusion models, studying the simple cases where  $p_X$  is a single Dirac mass or mixture of Dirac masses. We depart from these simple scenarios by showing that **blind denoisers can estimate noise levels from images, assuming low intrinsic dimensionality of the underlying data distribution**. We provide complete, rigorous derivations (e.g., sampling guarantees) under this assumption, in addition to numerical experiments.

### Sample complexity of diffusion models

Chen et al. (2023) and Lee et al. (2023) were among the first to provide a discretization analysis of (non-blind) denoising diffusion models specialized to the SDE case. They showed that sufficiently well-approximated score functions (equivalently, our assumption **(A3)** below) can sample from a target distribution in polynomial time. A flurry of works swiftly followed, hoping to improve the bounds initially published in these works. For example, Benton et al. (2024) and Conforti et al. (2025) both proposed using time-dependent noise schedules to obtain a tighter dimension dependence. A subsequent line of work has shown that sampling guarantees for non-blind denoising diffusion models scales with the *intrinsic* dimensionality of the data, not the ambient dimension, corresponding to our **(A2)** (Huang et al., 2024; Li and Yan, 2024; Potapchik et al., 2024). Fundamentally our results are incomparable as these works all study non-blind denoising diffusion models.

### Notation

We denote the centered Gaussian with variance  $\sigma^2 > 0$  as  $\gamma_{\sigma^2} = \mathcal{N}(0, \sigma^2 I)$ . Throughout, we denote the data distribution as  $p_X$ , and the noisy data distribution(s) as  $p_\sigma = p_X * \gamma_{\sigma^2}$ . We let  $dB_t$  denote standard Brownian motion. We use  $a \lesssim b$  (resp.  $a \gtrsim b$ ) to mean that there exists a constant  $C$  such that  $a \leq Cb$  (resp. a constant  $c$  such that  $a \geq cb$ ). If both  $a \lesssim b$  and  $b \lesssim a$ , then we write  $a \asymp b$ . We use, for example,  $a \lesssim_{\log} b$  to ignore logarithmic factors (in  $b$ ). Finally, a ball of radius  $R > 0$  centered at  $a \in \mathbb{R}^d$  is denoted by  $B(a, R)$ .

## 2 Preliminaries

### 2.1 Primer on variance exploding diffusion models

We first briefly review background material on *variance-exploding* (VE) diffusion models.

For a fixed terminal time  $T > 0$  and diffusion schedule  $(a_t)_{t \in [0, T]}$  with  $a_t \geq 0$ , consider the forward noising SDE

$$dX_t = \sqrt{2a_t} dB_t,$$

where  $X_0 \sim p_X$ . Then,  $\text{Law}(X_t) = p_{\sigma_t} = p_X * \gamma_{\sigma_t^2}$ , where  $\sigma_t^2 = 2 \int_0^t a_s ds$ . Following the theory of SDEs (Föllmer, 1985), the time-reversed process can be written as

$$dX_t^\leftarrow = -a_t \nabla \log p_{\sigma_{T-t}}(X_t^\leftarrow) dt + \sqrt{2a_t} dB_t,$$

where now  $X_t^\leftarrow := X_{T-t} \sim p_{\sigma_{T-t}}$ .

The reverse process above is driven by  $\nabla \log p_{\sigma_t}$ , known as the *score function*. A standard calculation known as Tweedie's formula (Miyasawa, 1961; Efron, 2011; Raphan and Simoncelli, 2011) relates the score to the posterior mean:

$$s_{\sigma_t}^*(y) := \sigma_t^2 \nabla \log p_{\sigma_t}(y) = \mathbb{E}[X|Y=y] - y, \quad (5)$$

where we take the conditional expectation of  $X$  given  $Y$  in the model  $X \sim p_X$ ,  $Y \sim \mathcal{N}(X, \sigma_t^2 I)$ . In other words, the score function of  $p_Y$  is proportional to the difference between the *denoiser* (the posterior mean  $\mathbb{E}[X|Y=y]$ ), and the noisy sample  $y$ .

## 2.2 Training and sampling with blind denoisers

Unlike standard denoisers in the diffusion model literature, blind denoiser are not given the noise level during training. Letting  $f_\theta : \mathbb{R}^d \rightarrow \mathbb{R}^d$  denote a neural network, a *blind denoiser* is trained using the following objective:

$$\hat{f}_\theta = \operatorname{argmin}_\theta \frac{1}{n} \sum_{i=1}^n \mathbb{E}_{\substack{\sigma \sim \Theta \\ z \sim \gamma}} \|\mathbf{x}_i - f_\theta(\mathbf{x}_i + \sigma z)\|^2 \quad (6)$$

where  $\{\mathbf{x}_i\}_{i=1}^n \sim p_X$  are the clean training samples,  $\gamma$  is the standard Gaussian in  $\mathbb{R}^d$ , and  $\Theta$  is a prior distribution over noise levels in the range  $[\sigma_T, \sigma_0]$ , with  $0 < \sigma_T < \sigma_0 < +\infty$ . (Since we are interested in the reverse process,  $\sigma_0$  is the largest noise level, and  $\sigma_T$  is the smallest.) In practice, we minimize (6) using (batch) stochastic gradient descent, see Algorithm 1 for pseudocode.

To sample, we initialize  $Y_0 \sim \mathcal{N}(0, \sigma_0^2 I)$  and consider various discretizations of

$$dY_t = (\hat{f}_\theta(Y_t) - Y_t) dt + \sqrt{2a_t} dB_t; \quad (7)$$

see Algorithm 2. For example, a standard Euler discretization results in

$$Y_{(k+1)h} = Y_{kh} + h(\hat{f}_\theta(Y_{kh}) - Y_{kh}) + \mathcal{N}(0, 2a_t h I),$$

where  $h > 0$  is a constant step size, and  $(a_t)_{t \geq 0}$  is a predetermined diffusion coefficient schedule. We additionally discuss the exponential (Euler) integrator in Appendix C.1, as it plays a role in our analysis.

## 3 Theoretical contributions

This section contains our theoretical contributions, which rigorously justify the use of BDDMs as generative models. All proofs are provided in the appendix.

### 3.1 The optimal blind denoiser

The first step is to understand the population minimizer of the blind denoising problem (6): Given infinite data and perfect optimization, what is (6) learning? Since the noise level is not known, it should be treated as a random variable as opposed to a known parameter. From a Bayesian perspective, the optimal solution then comes from marginalizing over this random variable. The following theorem makes this precise and indicates that the optimal blind denoiser can be expressed as a *conditional average* of score functions.

#### Proposition 3.1: Optimal blind denoiser

The population minimizer of (6) is

$$f^* : y \mapsto y + \int \sigma^2 \nabla \log p_\sigma(y) d\mu(\sigma|y),$$

where  $p_\sigma := p_X * \mathcal{N}(0, \sigma^2 I)$ , and

$$\mu(\sigma|y) \propto \frac{\Theta(\sigma)}{\sigma^d} \mathbb{E}_{X \sim p_X} [\exp(-\frac{\sigma^{-2}}{2} \|X - y\|^2)]. \quad (8)$$

We can thus- express the optimal blind score function as an integral over the mixture, i.e.,

$$s^*(y) := f^*(y) - y = \int \sigma^2 \nabla \log p_\sigma(y) d\mu(\sigma|y). \quad (9)$$

### 3.2 Derivation of the implicit noise schedule

We now examine the dynamics arising from the optimal blind score function (9). To start, we consider the continuous-time analogue of the dynamics suggested by the algorithm of Kadkhodaie and Simoncelli (2020) with a perfectly trained denoiser, which are given by

$$dX_t^* = s^*(X_t^*) dt + \sqrt{2a_t} dB_t \quad (10)$$

where we initialize with  $X_0^* \sim \mathcal{N}(0, \sigma_0^2 I)$ .

We consider the following ansatz: for all  $t$ ,  $X_t^*$  is approximately distributed as  $p_{\sigma_t}$ , for some denoising schedule  $(\sigma_t)_{t \geq 0}$  (to be derived). Further, let us suppose that when  $y = X_t^*$ , then the conditional distribution  $\mu(\sigma|X_t^*)$  in (8) concentrates on the true noise level  $\sigma_t$ . By (9), this suggests considering the following process in which we replace the conditional average over noise levels with  $\sigma_t$ :

$$dX_t = s_{\sigma_t}^*(X_t) dt + \sqrt{2a_t} dB_t := (\sigma_t^2 \nabla \log p_{\sigma_t}(X_t)) dt + \sqrt{2a_t} dB_t. \quad (11)$$

However, along (11), the evolution of the density is given by SDE theory, in particular by the Fokker–Planck equation. In order to be consistent with the ansatz  $\text{Law}(X_t) \approx p_{\sigma_t}$ , this implies the following ODE for  $\sigma_t$  (see Appendix A.2):

$$\sigma_t \dot{\sigma}_t = -\sigma_t^2 + a_t. \quad (12)$$

Solving this ODE, we arrive at the following result.

### Proposition 3.2: Implicit noise schedule

The ideal dynamics (11) satisfies  $\text{Law}(X_t) = p_{\sigma_t}$  for all  $t \geq 0$ , provided that

$$\sigma_t^2 = \sigma_0^2 e^{-2t} + 2 \int_0^t a_s e^{-2(t-s)} ds.$$

We record two properties of this noise schedule.

**Lemma 3.3.** *If  $t \mapsto a_t$  is decreasing and  $a_0 \leq \sigma_0^2$ , then  $t \mapsto \sigma_t$  is decreasing.*

**Lemma 3.4.** *If  $t \mapsto a_t$  is decreasing and  $a_t \rightarrow 0$  as  $t \rightarrow \infty$ , then  $\sigma_t \rightarrow 0$  as well.*

Henceforth, we assume that the conditions of Lemma 3.4 hold. In brief, this discussion suggests that if  $\mu(\cdot|X_t)$  concentrates around  $\sigma_t$  such that

$$\int \sigma^2 \nabla \log p_\sigma(y) d\mu(\sigma|X_t) \approx \sigma_t^2 \nabla \log p_{\sigma_t}(X_t), \quad (13)$$

and if  $a_t \rightarrow 0$ , then heuristically we expect  $\text{Law}(X_t^*) \approx \text{Law}(X_t) \rightarrow p_X$  as  $t \rightarrow \infty$ .

We stress that at no point during the sampling process will the blind denoiser be given information about the schedule  $\sigma_t$ . Instead, it must adapt to this schedule automatically by estimating  $\sigma_t$  from the current input  $Y_t$ . In other words, if  $\mu(\sigma|X_t)$  concentrates, the  $\sigma_t$  for which  $p_{\sigma_t} = p_X * \mathcal{N}(0, \sigma_t^2 I)$  can be inferred from input  $Y_t$ . This is because  $p_\sigma(Y_t)$  would be negligible for all  $\sigma$  but a small set around  $\sigma_t$ . As a result, the ideal dynamics in the backward process should follow the true schedule  $\sigma_t$  given above.

### 3.3 Error bound without discretization

Suppose now that we have an empirical minimizer  $\hat{f}_\theta$  that will act as the blind denoiser, and let  $\hat{p}_t := \text{Law}(Y_t)$  along the trained dynamics (7). For now, we omit discretization error, deferring this discussion to Section 3.5. Our goal is to bound the KL divergence between  $\hat{p}_T$ , the distribution corresponding to our algorithm at time  $T$ , and the target distribution with some small additional noise  $p_{\sigma_T} = p_X * \mathcal{N}(0, \sigma_T^2 I)$ .

By a standard application of Girsanov's theorem, we can decompose this error into the following terms using the triangle inequality:

$$\text{KL}(p_{\sigma_T} \| \hat{p}_T) \lesssim \text{KL}(p_{\sigma_0} \| \hat{p}_0) + \int_0^T \frac{1}{a_t} (\|\hat{f}_\theta - f^*\|_{L^2(p_{\sigma_t})}^2 + \|s_{\sigma_t} - s^*\|_{L^2(p_{\sigma_t})}^2) dt. \quad (14)$$

The first term on the right-hand side corresponds to the initialization error. The second term measures how close the trained denoiser is to the optimal one (the “score error”). Finally, the third term is related to the error in the approximation (13), i.e., the error in estimating the noise level. This last term is the primary novelty over prior work on diffusion models, so we focus our attention on it.

Before stating our main results, we require the following assumptions and definitions. The support of our data distribution will be denoted by  $\mathcal{X} := \text{supp}(p_X)$ , and we let  $\mathbf{k}$  denote the “[intrinsic dimension](#)” of  $p_X$ , defined as follows.

**Definition 3.5** (Intrinsic dimension). If  $p_X$  has support  $\mathcal{X}$ , we define the *intrinsic dimension* of  $p_X$  at scale  $r_0$  to be  $\mathbf{k} := 1 + \log N_{\mathcal{X}}(r_0)$ , where  $N_{\mathcal{X}}(r_0)$  denotes the minimal number of balls of radius  $r_0$  needed to cover  $\mathcal{X}$ .

For example, if  $\mathcal{X}$  is a  $k$ -dimensional subspace and  $\mathcal{X}$  has diameter  $R$ , then  $k \asymp k \log(R/r_0)$ . But the [intrinsic dimension captures a broader range of situations](#) such as manifold structure, or when  $\mathcal{X}$  is actually full-dimensional but resembles a  $k$ -dimensional manifold at scale  $r_0$ . Our proofs require  $r_0 = \sigma_T^2/(\sigma_0\sqrt{d})$  as the choice of scale.

Our assumptions are the following.

- (A1)  $\mathcal{X} \subset B(0, R)$  for some  $R > 0$ .
- (A2)  $p_X$  has low intrinsic dimensionality, with  $k^2 \ll \log d$ .
- (A3) For  $\varepsilon_{\text{BD}} > 0$ ,  $\int_0^T a_t^{-1} \|\hat{f}_\theta - f^*\|_{L^2(p_{\sigma_t})}^2 dt \leq \varepsilon_{\text{BD}}^2$ .

Note that (A1), (A2), and (A3) are relatively mild. In particular, (A2) is inspired from empirical observations (Olshausen and Field, 1996; Roweis and Saul, 2000; Chandler and Field, 2007; Hénaff et al., 2014; Pope et al., 2021; Brown et al., 2023) and has been leveraged in several other works on sampling via diffusion models (Li and Yan, 2024; Pooladian and Niles-Weed, 2025; Liang et al., 2025). (A3) is analogous to the standard assumption that the score functions are accurately learned in  $L^2$ . In its current form, it is somewhat obscure; we provide further discussion in Section 3.7 when we specialize to specific noise schedules.

We are now in a position to state our first main result.

#### Theorem 3.6: Error bound without discretization

Under (A1)–(A3), the KL divergence between the (reverse) processes (7) and (11) is bounded by

$$\text{KL}(p_{\sigma_T} \| \hat{p}_T) \lesssim_{\log} \frac{R^2}{\sigma_0^2} + \varepsilon_{\text{BD}}^2 + \frac{(R^2 + k)k^2}{d} A_T,$$

where  $A_T = \int_0^T (a_t)^{-1} dt$ .

The first term (initialization error) is made small with a suitably large choice of  $\sigma_0^2$ , and the second term (the “score error”) is small if the training is successful. The third term, which scales with  $k$ , is discussed next.

### 3.4 Interpretation as a Bayesian problem

We now provide an overview of our proof with rigorous details deferred to the appendix. As the first two terms in Theorem 3.6 are standard, we focus on the novel term  $\int_0^T a_t^{-1} \|s_{\sigma_t} - s^*\|_{L^2(p_{\sigma_t})}^2 dt$  which captures the error in estimating the noise level.

Note that for  $X_t \sim p_{\sigma_t}$

$$\begin{aligned} \|(s_{\sigma_t}^* - s^*)(X_t)\|^2 &= \left\| \int \sigma^2 \nabla \log p_\sigma(X_t) d(\delta_{\sigma_t} - \mu(\sigma|X_t)) \right\|^2 \\ &= \left\| \iint_{\sigma}^{\sigma_t} \partial_\omega (\omega^2 \nabla \log p_\omega(X_t)) d\omega d\mu(\sigma|X_t) \right\|^2, \end{aligned}$$

where we used the fundamental theorem of calculus in the last line. A simple calculation shows that

$$\partial_\omega (\omega^2 \nabla \log p_\omega(y)) = \omega^{-3} \text{Cov}_{q_\omega}(X, \|X - Y\|^2 | Y = y),$$

where under  $q_\omega$  we have  $X \sim p_X$ ,  $Y \sim \mathcal{N}(X, \omega^2 I)$ . We show in Proposition B.1 that the conditional covariance is bounded in terms of the intrinsic dimension  $k$ , essentially leading to a bound on the above term of order

$$(R^2 + k) k^2 \sigma_t^4 \int |\sigma_t^{-2} - \sigma^{-2}|^2 d\mu(\sigma|X_t).$$

The remainder of the analysis is a frequentist analysis of a Bayesian method: We have an observation  $X_t \sim p_{\sigma_t}$ , where  $\sigma_t$  is the “ground truth” noise level. We ask whether the posterior distribution on the noise level  $\mu(\cdot|X_t)$  concentrates on  $\sigma_t$  given a single sample. For interpretability, we focus on the class of power law priors  $\Theta(\sigma) \propto \sigma^{\alpha-3}$  on  $[\sigma_T, \sigma_0]$  for  $\alpha \in \mathbb{R}$ , and we use the following change of variables.

**Lemma 3.7.** *If  $\sigma \sim \mu(\cdot|y)$  in (8), then  $\lambda := \sigma^{-2}$  is distributed according to*

$$\nu(\lambda|y) \propto \lambda^{(d-\alpha)/2} \mathbb{E}_{X \sim p_X} [\exp(-\frac{\lambda}{2} \|X - y\|^2)]. \quad (15)$$

Writing  $\ell(\lambda|y) := -\log \nu(\lambda|y)$ , then

$$\begin{aligned} \ell'(\lambda|y) &= -\frac{d-\alpha}{2\lambda} + \frac{1}{2} \mathbb{E}_{q_\lambda} [\|X - Y\|^2 | Y = y], \\ \ell''(\lambda|y) &= \frac{d-\alpha}{2\lambda^2} - \frac{1}{4} \text{Var}_{q_\lambda} (\|X - Y\|^2 | Y = y), \end{aligned}$$

where, in an abuse of notation, we use  $q_\lambda$  to denote the joint distribution for which  $X \sim p_X$ ,  $Y \sim \mathcal{N}(X, \lambda^{-1} I)$ .

Notice that there is no reason for  $\ell''(\cdot|y)$  to always be convex, given the presence of a negative sign on the second term. However, our low intrinsic dimensionality assumption **(A2)** nevertheless allows us to show that the noise variance posterior concentrates on the ground truth signal  $\lambda_t := \sigma_t^{-2}$ .

### Proposition 3.8: Estimating the noise level

Under **(A1)**–**(A2)**, for  $X_t \sim p_{\sigma_t}$ ,  $\lambda \sim \nu(\cdot|X_t)$ ,

$$\mathbb{E}|\lambda - \lambda_t|^2 \lesssim_{\log} \lambda_t^2 (d^{-1} + k^2 d^{-2}).$$

Combining these the ingredients yields the claimed bound on the noise level term.

## 3.5 Discretization, noise, and step size schedules

**A family of convenient diffusion schedules.** Although our results apply to general choices of  $(a_t)_{t \geq 0}$ , for the sake of exposition we specialize to a particular convenient family in order to state our next results in a more interpretable form. Namely, if we take  $a_t = a\sigma_t^2$  for some  $a \in (0, 1)$ , then the ODE (12) becomes particularly easy to solve:  $\sigma_t = \sigma_0 e^{-(1-a)t}$ . We henceforth fix this particular schedule.

**Discretization error.** If the SDE (7) is discretized, then in addition to the error terms present in Theorem 3.6, we will also incur a discretization error. In order to establish an iteration bound which also scales with the intrinsic dimension, we consider the exponential Euler integrator (see Appendix C.1). With this choice, the discretization

error takes the following form: Writing  $t_- := \lfloor t/h \rfloor h$  where  $h$  is the step size, thus  $N = T/h$  is the total number of iterations,

$$\text{Disc}(h) = \int_0^T a_t^{-1} \mathbb{E} \|f_{\sigma_{t_-}}^*(X_{t_-}) - f_{\sigma_t}^*(X_t)\|^2 dt.$$

(Indeed  $\text{Disc}(h)$  arises from (14) if we also incorporate discretization error.) Here,  $f_\sigma^*$  denotes the Bayes denoiser when the noise level is known:  $f_\sigma^*(y) := \mathbb{E}_{q_\sigma}[X|Y=y]$ . We analyze the discretization error and establish the following bound.

**Theorem 3.9: Discretization error**

Under **(A1)–(A3)** and with the exponential Euler scheme,

$$\text{Disc}(h) \lesssim_{\log} R^2 \sigma_T^{-2} k^3 h^2 \mathbf{1}_{a \neq 1/2} + k^2 h.$$

Remarkably, the first error term vanishes *exactly* when  $a = 1/2$ . Therefore, our analysis reveals a canonical choice of noise schedule, namely  $a_t = \sigma_0^2 e^{-t}/2$ , which leads to smaller discretization error.

Moreover, if  $a = 1/2$ , the error bound shows that we can provably choose a constant step size  $h$ , scaling with the intrinsic dimension  $k$ . This is in stark contrast to theoretical guarantees for the variance-preserving DDPM algorithm, which requires carefully tuned exponentially decaying step sizes to compensate for the singularity of the score for time  $t \rightarrow T$  (Benton et al., 2024; Conforti et al., 2025).

### 3.6 Sampling in a “perceptual” metric

At this point, we nearly have a complete sampling guarantee for BDDMs. However, Theorem 3.6 only guarantees closeness to  $p_{\sigma_T} = p_X * \mathcal{N}(0, \sigma_T^2 I)$ , not to  $p_X$ . One approach is to simply assume that sampling from  $p_{\sigma_T}$  is our goal all along for some small  $\sigma_T$ , which is sometimes adopted in the literature (Gatmiry et al., 2026).

More commonly,  $p_{\sigma_T}$  is used as a technical device to sample from  $p_X$ , which is known as *early stopping*. How small do we need to take  $\sigma_T$  in order to ensure that  $p_{\sigma_T}$  and  $p_X$  are close? This is important, since both the noise estimation error (via  $A_T$ ) and the discretization error depend on  $\sigma_T^{-1}$ . Existing theory takes  $\sigma_T \asymp \varepsilon/\sqrt{d}$  to ensure that  $p_X$  and  $p_{\sigma_T}$  are  $\varepsilon$ -close in the Wasserstein metric—this is insufficient for us as we expect  $d \gg 1$ .

We instead propose the following pseudo-metric:

$$D_{\mathcal{X}}(p, q) := \sup \{ \mathbb{E}_p[f \circ \Pi_{\mathcal{X}}] - \mathbb{E}_q[f \circ \Pi_{\mathcal{X}}] : f \in \text{BLip} \},$$

where  $\Pi_{\mathcal{X}}$  is the projection operator onto  $\mathcal{X} = \text{supp}(p_X)$ , and  $\text{BLip}$  is the space of 1-bounded, Lipschitz functions.\* A natural interpretation of this metric is that it corresponds to “perceptual differences” and ignores orthogonal information. We show that closeness in  $D_{\mathcal{X}}$  is implied by taking  $\sigma_T \asymp \varepsilon/\sqrt{k}$ , depending on the intrinsic dimension. Leveraging this, we provide the following full convergence guarantee.

\*Functions which are 1-Lipschitz and with  $-1 \leq f \leq 1$ .

### Corollary 3.10: Full BDDM convergence guarantee

Assume **(A1)–(A3)** and let  $p_{\text{alg}}$  be the output of BDDM with exponential Euler discretization. Let  $a_t = \sigma_0^2 e^{-t}/2$ ,  $\sigma_T \asymp_{\log} \varepsilon/\sqrt{k}$ ,  $\sigma_0 \asymp \varepsilon/R$ , and  $h \asymp_{\log} \varepsilon^2/k^2$ . Then,  $D_{\mathcal{X}}(p_X, p_{\text{alg}}) \lesssim \tilde{\varepsilon}_{\text{BD}} + \varepsilon$ , provided

$$d \gg_{\log} (R^2 + k) k^3 \varepsilon^{-4} \quad \text{and} \quad N \asymp_{\log} k^2 \varepsilon^{-2}.$$

In this result, the definition of the score error has to be slightly modified to  $\tilde{\varepsilon}_{\text{BD}}^2 := \int_0^T a_t^{-1} \|\widehat{f}_\theta - f^*\|_{L^2(p_{\sigma_t})}^2 dt$ , since the error only matters at discretization time steps.

*Remark 3.11.* The use of the word “perceptual” is merely suggestive. We imagine that features (of images captured by neural networks) implicitly playing the role of the low intrinsic dimensionality of the data. We stress that a rigorous development of a meaningful metric (beyond the commonly used Fréchet Inception Distance aka FID) to quantify diversity and quality is of immense interest but far outside the scope of this work.

## 3.7 On the choice of noise prior

Finally, we revisit the assumption **(A3)** on the “score estimation error”. In standard DDPM theory, the bound on the score estimation error in  $L^2$  which is needed for the discretization analysis can also be written as the *excess risk* of the population score matching loss. This leads to a remarkable harmony between statistical theory which can identify when the  $L^2$  error is small, and the discretization analysis. In the context of the convenient noise schedules defined above, we prove the analogous result for BDDMs.

### Theorem 3.12: Score estimation error

Suppose that  $[\sigma_T, \sigma_0] \subseteq \text{supp } \Theta$ . It holds that

$$\varepsilon_{\text{BD}}^2 \leq \left( \min_{\sigma_T \leq \sigma \leq \sigma_0} a(1-a) \sigma^3 \Theta(\sigma) \right)^{-1} \mathcal{E}(\widehat{f}_\theta),$$

where  $\mathcal{E}(\cdot)$  denotes the population excess risk for (6).

This result shows that if the neural network learns a good blind denoiser, in the sense of attaining a small excess risk, then the  $\varepsilon_{\text{BD}}$  quantity in our error analysis is controlled. Moreover, [our analysis singles out a particularly good choice of noise prior](#). Namely, when  $\Theta(\sigma) \propto \sigma^{-3}$  over  $[\sigma_T, \sigma_0]$ , then  $\varepsilon_{\text{BD}}^2$  and  $\mathcal{E}(\widehat{f}_\theta)$  are in fact equal up to a constant, so that the training objective and the error propagation along the dynamics are well-aligned.<sup>†</sup> Although we state this for a particular family of noise schedules for concreteness, the same approach indeed identifies a well-aligned prior  $\Theta$  for each schedule  $(a_t)_{t \geq 0}$ .

## 4 Empirical results

We now present several experiments on both synthetic and photographic image datasets which corroborate our theoretical findings. In particular, these experiments demonstrate that in practice: (1) the noise variance can be accurately estimated from a single

<sup>†</sup>Note that  $\Theta(\sigma) \propto \sigma^{-3}$  corresponds to a uniform prior over  $\lambda$ .

---

**Algorithm 1** Training a blind denoiser

---

**Input:** Distribution  $\Theta$ , neural network  $f_\theta$

**while** not converged **do**

- Draw  $x_1, \dots, x_B \sim p_X$
- Draw  $\sigma_1, \dots, \sigma_B \sim \Theta$
- Draw  $z_1, \dots, z_B \sim \mathcal{N}(0, I)$
- Compute  $\mathcal{L}(\theta) = B^{-1} \sum_{i=1}^B \|x_i - f_\theta(x_i + \sigma_i z_i)\|^2$
- Update  $\theta^+ \leftarrow \theta - \eta \nabla_\theta \mathcal{L}(\theta)$ .

**end while**

---

**Algorithm 2** Sampling using a blind denoising model

---

**Input:** Trained neural network  $\hat{f}_\theta$ , stepsize  $h > 0$ , diffusion coefficients  $(a_t)_{t \in [0, T]}$ , and  $\sigma_{\max}, \sigma_{\min} > 0$

**Initialize**  $X_0 \sim \mathcal{N}(\hat{m}_X, \sigma_{\max}^2 I)$ ,  $k = 0$

**while** keepgoing == True **do**

- $s_k = f_\theta(X_{kh}) - X_{kh}$
- Compute  $\hat{\sigma}_k^2 \leftarrow \|s_k\|^2/d$
- if**  $\hat{\sigma}_k \leq \sigma_{\min}$  **then**

  - keepgoing  $\leftarrow$  False

- else**

  - Draw  $\xi \sim \mathcal{N}(0, \int_{kh}^{(k+1)h} 2a_t dt)$
  - Update  $X_{(k+1)h} \leftarrow X_{kh} + hs_k + \xi$

- end if**

**end while**

---

noisy observation in high dimensions; (2) the backward process of Algorithm 2 closely adheres to the theoretical implicit schedule of Proposition 3.2; (3) BDDMs can offer a substantial gain in sampling performance compared to non-blind models, by eliminating the mismatch between true noise level and a proposed noise schedule.

## 4.1 Blind denoisers on synthetic data

As we proved in Section 3, when  $\mu(\sigma|x_\sigma)$  concentrates around the true noise level, the optimal blind denoiser converges to and can be approximated by the non-blind denoiser (13). The approximation error decreases as the gap  $k^2 \ll d$  widens. We first ask if the noise level can be accurately estimated from a noisy observation in practice. In this section, we empirically verify these claims on toy data.

### Analytical blind denoisers

We first study an analytical blind denoiser model when  $p_X$  is a 2-component mixture of Gaussians supported on a  $k$ -dimensional subspace in  $\mathbb{R}^d$ . Here, the optimal score function  $\nabla \log p_\sigma$  is known in closed form, allowing us to isolate the error induced by the uncertainty in noise estimation. Our analytical blind denoiser will be given by a

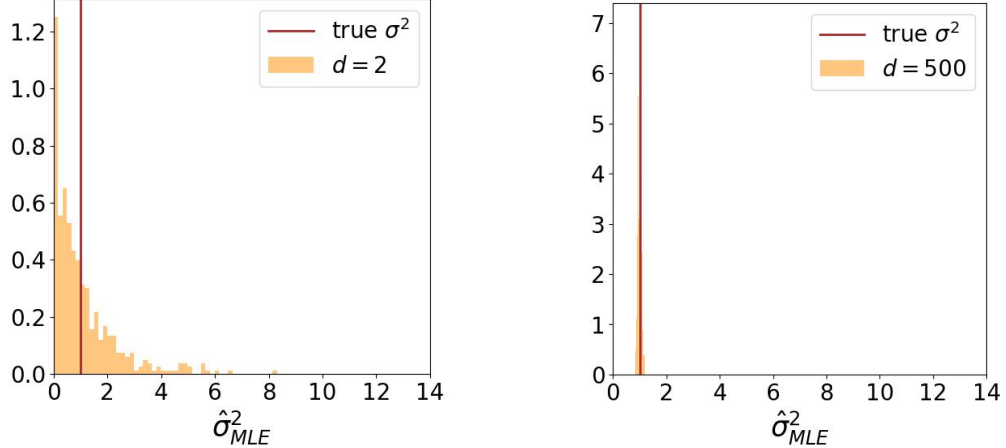


Figure 1: Empirical density of maximum likelihood noise level estimates  $\hat{\sigma} = \arg \max \mu(\sigma|y)$  for a mixture of two Gaussians with intrinsic dimensionality  $k = 2$  in an ambient space of dimensionality  $d$ . Estimates are broadly distributed when  $d = k$  (**left**), but highly concentrated when  $d \gg k^2$  (**right**).

maximum likelihood estimate (MLE) of  $\mu(\cdot|y)$  for a noisy sample  $y$ :

$$s^*(y) \approx \hat{s}(y) := \hat{\sigma}^2 \nabla \log p_{\hat{\sigma}}(y), \quad \hat{\sigma} = \arg \max \mu(\sigma|y)$$

Figure 1 shows the distribution of estimated noise values for a mixture of two Gaussians of dimensionality  $k$  in a  $d$ -dimensional ambient space. Estimates are broadly distributed when  $k \approx d$ , but concentrate when  $k^2 \ll d$ , illustrating a “blessing of dimensionality”. Figure 2 shows samples generating via Algorithm 2 using our analytical denoiser. In these experiments,  $h = 0.3$  and the dynamics are deterministic ( $a_t = 0$ ). Similar results are obtained when  $a_t > 0$ . For more details, see Appendix G.1.

### Training denoisers on synthetic data

In Appendix G.2, we verify that training blind denoisers (via neural networks) can accurately sample from toy densities as well. Under an appropriate step-size choice of  $h = 0.5$  and  $a_s = \frac{1}{2}\sigma_t^2$ , we see that  $\hat{\sigma}_k \simeq \sigma_t$  as predicted by Proposition 3.2. Figure 3 demonstrates the benefits of having low intrinsic dimensionality for learning to sample Gaussian data, and similarly for Gaussian mixtures (see appendix for training details).

## 4.2 Photographic images

Do these results extend beyond the synthetic data to real-world models and signals? To investigate this question, we consider deep neural networks trained on natural images. We trained a non-blind and blind model to approximate the optimal denoisers in (5) and (9), respectively.

**Datasets.** Under the manifold hypothesis, natural images concentrate near a union of low-dimensional manifolds. This implies that natural images have low intrinsic dimensionality, making them a suitable testbed for our theoretical results. We use two popular image datasets, CelebA (Liu et al., 2015) with  $\approx 200,000$  images and a random subset of LSUN (bedroom class) data set with  $\approx 300,000$  images (Yu et al., 2015).

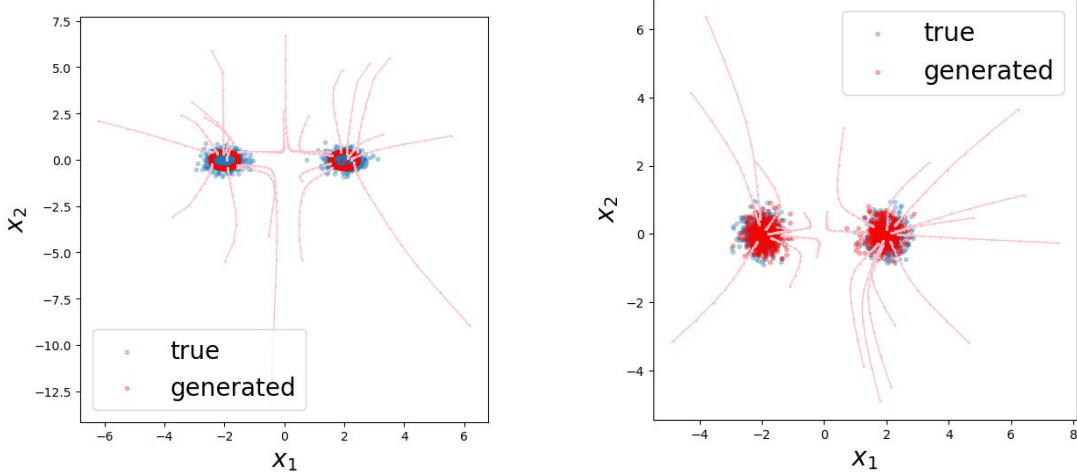


Figure 2: Example trajectories and samples for an analytical blind denoiser applied to a mixture of two Gaussians with  $k = 2$ . For  $d = k = 2$  (left), sampling fails, due to errors in the MLE estimates of noise level. For  $d = 500 \gg k^2$  (right), sampling is successful, illustrating the blessings of dimensionality.

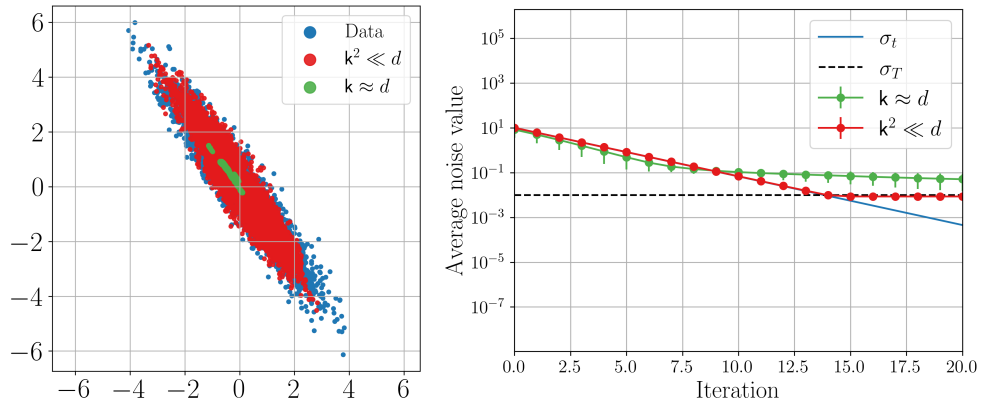


Figure 3: Sampling performance of BDDMs trained on Gaussian data with intrinsic dimension  $k = 2$  and two different input dimensions  $d \in \{2, 100\}$ . Generated samples (left) and evolution of the estimated noise level, corresponding to Proposition 3.2 (right).

These datasets are complex enough to capture real-world structure while remaining simple enough to train smaller-size networks without text conditioning. All images are downsampled to  $80 \times 80$  resolution.

**Architecture and training.** UNet (Ronneberger et al., 2015) is the most popular denoising and score estimation architecture. For both blind and non-blind models, we use the simplest UNet architecture with 13 million parameters, and train all models from scratch. (We note that this architecture is quite small compared to others which use hundreds of millions of parameters). See Appendix G.3 for more details.

Can the noise level be accurately estimated from a single noisy image by a trained neural network denoiser? If natural images are truly low dimensional, then we expect  $\mu(\sigma|x_\sigma) \simeq \delta_\sigma$ . Additionally, the inductive biases of the neural network should allow for leveraging the concentration to get a precise estimate of true variance. If both of

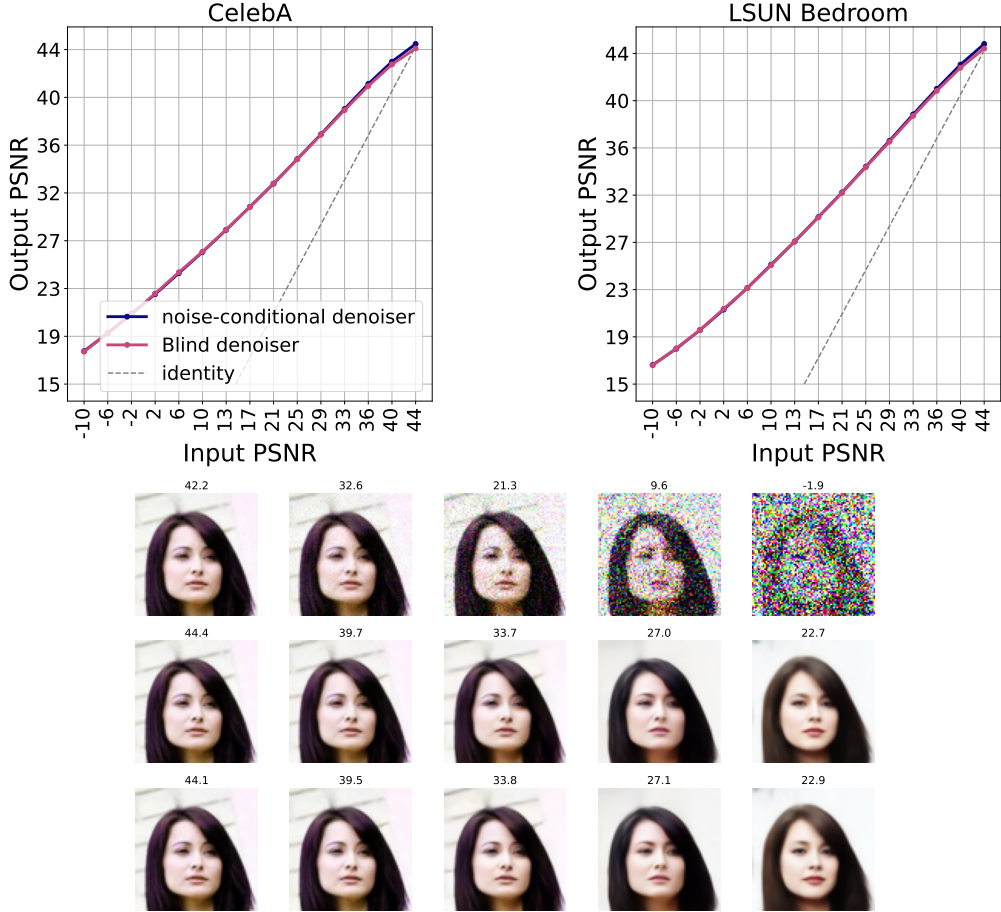


Figure 4: **Top panel.** Comparison of denoising performance of blind and non-blind denoisers. Performance is evaluated on the test sets of CelebA and Bedroom class of LSUN datasets, and is reported in terms of PSNR. For consistency, the noise level on the horizontal axis is also expressed as  $\text{PSNR}(x, x_\sigma)$ . **Bottom panel.** An example test image with corresponding PSNR values. **Top:** Noisy images. **Middle:** Denoised image by a non-blind denoiser. **Bottom:** Denoised image by a blind denoiser.

these conditions are satisfied, then the performance gap between blind and non-blind denoisers will be small. Figure 4 compares denoising error of the two models on two datasets in terms of their peak signal-to-noise ratio (PSNR) averaged across the data, written  $\text{PSNR}(x, \hat{x}) := -10 \log_{10} \|x - \hat{x}\|^2$ , where  $\hat{x}$  is the output of a blind or non-blind denoiser. The two plots clearly display that both blind and non-blind denoisers have the same “one-shot” denoising ability, as their denoising errors are virtually identical.

Now we sample from  $\hat{p}_T \approx p_X$  learned by the models via Algorithm 2. Hyperparameters are set to  $\sigma_{\max} = 4$ ,  $\sigma_{\min} = 0.05$ ,  $h = 0.2$ ,  $a_t = 0.2\hat{\sigma}_t$ , which leads to a total number of steps  $N \approx 100$ . We compare to the non-blind denoisers through the variance exploding (VE) DDPM algorithm (Song et al., 2021a), with a  $\log \sigma$  schedule with  $N = 100$ .

Figures 5 shows samples from both algorithms (see Figure 7 for additional examples and Figure 8 for LSUN samples). Surprisingly, samples generated by BDDMs appear to have higher visual quality than samples generated by the non-blind DDMs. This suggests that the distribution of BDDM samples is closer to the true image density than that of DDPM samples.



Figure 5: Comparison of samples from BDDM and VE-DDPM. **Top row:** Randomly selected subset of training images from the celebA dataset. **Second row:** Samples generated by BDDM with  $N \approx 100$ . **Third row:** Samples generated by a non-blind DDM (VE-DDPM) with  $N = 100$ . Samples in each column are initialized with the same random seed, and use matched injected noise. Seeds are random and *not curated for quality*.

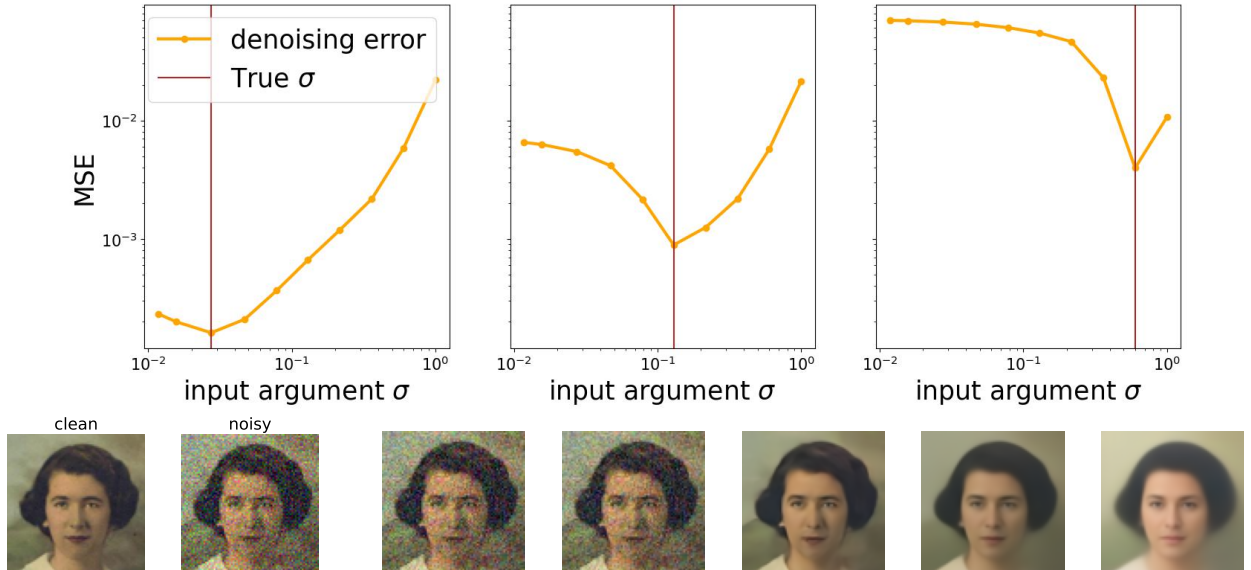


Figure 6: Sensitivity of non-blind denoising performance to mismatches in true noise level and argument to the denoiser. **Top row:** Denoising error (averaged over 512 samples) as a function of argument  $\sigma$  for three different true noise levels (from left to right,  $\sigma^* \in [0.025, 0.15, 0.6]$ ). **Bottom row:** Example clean image  $x_0$ , noisy image  $x_{\sigma^*} = x_0 + \sigma^* z$ , for  $\sigma^* = 0.1$ , and five images resulting from a non-blind denoiser  $\tilde{x} = \tilde{f}_\theta(x_{\sigma^*}, \sigma)$  with  $\sigma \in [0.01, 0.03, 0.10, 0.32, 1.0]$  (from left to right).

We hypothesize that using non-blind models in a backward process with an explicit schedule incurs a mismatch error: the “true” noise level on the image diverges from the noise level dictated by the schedule of the algorithm. Figure 6 illustrates the nature of the mismatch error in one-shot denoising in a non-blind model. Each plot shows the mean-squared error (MSE) between denoised and clean images, as a function of the second argument. MSE is lowest when the second argument is equal to the “true” noise level,  $\sigma = \sigma^*$ . If the argument  $\sigma$  is too small, the denoised image is noisier than that of the correct denoiser; too large, and the image is more blurred than that of the correct denoiser.



Figure 7: Higher number of steps  $N \approx 17000$  improves quality of samples for all models shown in Fig. 5. The samples from BDDM are still of significantly higher quality than samples from DDPM. Samples in each column are initialized with the same random seed with matched injected noise.



Figure 8: **Top row:** example training images from the LSUN dataste. **Second row:** samples generated by BDDM with average number of steps  $N \approx 1300$ . **Third row:** Samples generated by DDPM (VE) algorithm, with total number of steps  $N = 1300$ . Samples in each column are initialized with the same random seed with matched injected noise.

To quantify the mismatch in the DDPM backward sampling process, we train a separate small neural network to estimate the noise level of an image—a much simpler task than denoising. Figure 12 in the appendix shows that this network produces highly accurate estimates of noise level, confirming the concentration of the likelihood. We can use this network to estimate the true noise level of the intermediate samples generated by DDPM, and compare them to the  $\sigma$  imposed by the schedule.

Figure 9 shows that scheduled noise levels systematically fall behind the true noise value of the image. This suggests that the low quality of the samples in Figure 5 results from a mismatch error in which  $\sigma_t > \sigma^*$  along the trajectory. Per the left-most plot in Figure 9, this same noise-estimator model shows that, [BDDMs precisely track the implicit schedule of the backward process](#). Moreover, given our theoretical results, we can conclude that the only reason DDPM fails to generate images in the constant stepsize regime is precisely due to this mismatch which is not observed in BDDMs (see third row of Figure 5).

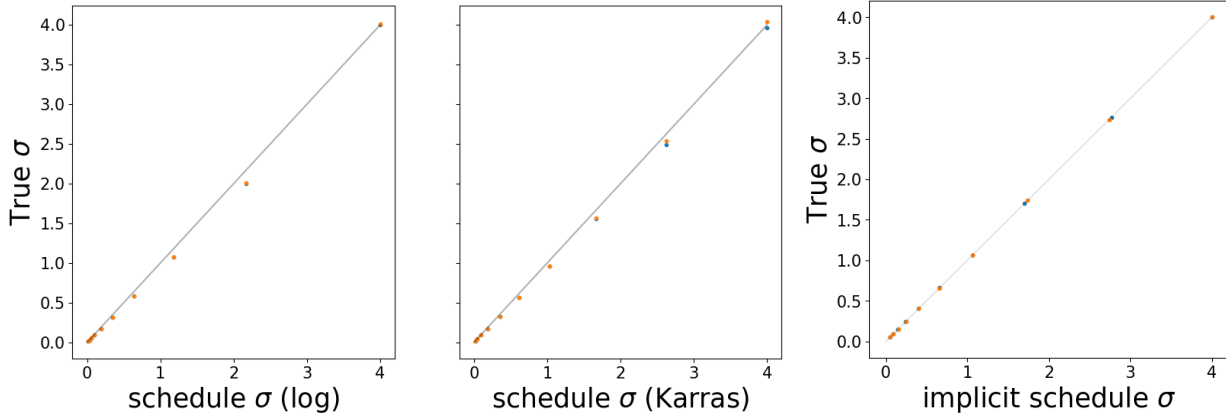


Figure 9: Empirical comparison of scheduled noise level  $\sigma_t$  and estimated noise level  $\sigma^*$  along trajectories of 50 steps for 2 samples. Every 5 steps is shown. The DDPM backward process outpaces a log schedule (left), or the schedule proposed by Karras et al. (2022) (middle), leading to an excess error manifested in the lower quality of samples. In contrast, BDDM accurately tracks the implicit schedule  $\sigma_t$  via  $\hat{\sigma}_k = \|x_k - \hat{f}_\theta(x_k)\|/\sqrt{d}$ . Adaptivity of step size to underlying sample is demonstrated. (right).

## 5 Conclusion

This work presents a comprehensive mathematical analysis and justification of blind denoising diffusion models, closing a gap in the literature. We identify *low intrinsic dimensionality* of the underlying data distribution, which allows the denoiser to (implicitly) estimate noise level from an image, as a critical component underlying the success of these models both theoretically and empirically. A key consequence is that, unlike e.g., DDPM, we prove that a constant stepsize schedule suffices to sample data distributions via BDDMs. Moreover, we have shown that BDDM models can offer improved sample quality by avoiding errors due to mismatch in noise schedules. The use of BDDMs merit further investigation at larger scales, as well as in application to other downstream tasks such as fine-tuning and inverse problems.

## Acknowledgements

ZK acknowledges the computing facilities of the Flatiron Institute. AAP acknowledges the Yale Institute for the Foundations of Data Science for financial support.

## References

Arjovsky, M., Chintala, S., and Bottou, L. (2017). Wasserstein generative adversarial networks. *Proceedings of the 34th International Conference on Machine Learning*, 70:214–223.

Benton, J., De Bortoli, V., Doucet, A., and Deligiannidis, G. (2024). Nearly  $d$ -linear convergence bounds for diffusion models via stochastic localization. In *The Twelfth International Conference on Learning Representations*.

Brown, B. C., Caterini, A. L., Ross, B. L., Cresswell, J. C., and Loaiza-Ganem, G. (2023). Verifying the union of manifolds hypothesis for image data. In *The Eleventh International Conference on Learning Representations*.

Chandler, D. M. and Field, D. J. (2007). Estimates of the information content and dimensionality of natural scenes from proximity distributions. *Journal of the Optical Society of America A*, 24(4):922–941.

Chen, F., Chewi, S., Daskalakis, C., and Rakhlin, A. (2026). High-accuracy sampling for diffusion models and log-concave distributions. *arXiv preprint 2602.01338*.

Chen, S., Chewi, S., Li, J., Li, Y., Salim, A., and Zhang, A. (2023). Sampling is as easy as learning the score: Theory for diffusion models with minimal data assumptions. In *The Eleventh International Conference on Learning Representations*.

Conforti, G., Durmus, A., and Silveri, M. G. (2025). KL convergence guarantees for score diffusion models under minimal data assumptions. *SIAM Journal on Mathematics of Data Science*, 7(1):86–109.

Efron, B. (2011). Tweedie’s formula and selection bias. *Journal of the American Statistical Association*, 106(496):1602–1614.

Föllmer, H. (1985). An entropy approach to the time reversal of diffusion processes. In *Stochastic differential systems (Marseille-Luminy, 1984)*, volume 69 of *Lect. Notes Control Inf. Sci.*, pages 156–163. Springer, Berlin.

Gatmiry, K., Chen, S., and Salim, A. (2026). High-accuracy and dimension-free sampling with diffusions. *arXiv preprint arXiv:2601.10708*.

Grathwohl, W., Chen, R. T. Q., Bettencourt, J., and Duvenaud, D. (2019). FFJORD: free-form continuous dynamics for scalable reversible generative models. In *International Conference on Learning Representations*.

Hénaff, O. J., Ballé, J., Rabinowitz, N. C., and Simoncelli, E. P. (2014). The local low-dimensionality of natural images. *CoRR*, abs/1412.6626.

Ho, J., Jain, A., and Abbeel, P. (2020). Denoising diffusion probabilistic models. *Advances in neural information processing systems*, 33:6840–6851.

Huang, Z., Wei, Y., and Chen, Y. (2024). Denoising diffusion probabilistic models are optimally adaptive to unknown low dimensionality. *arXiv preprint arXiv:2410.18784*.

Kadkhodaie, Z., Guth, F., Simoncelli, E. P., and Mallat, S. (2024). Generalization in diffusion models arises from geometry-adaptive harmonic representations. In *The Twelfth International Conference on Learning Representations*.

Kadkhodaie, Z. and Simoncelli, E. (2021). Stochastic solutions for linear inverse problems using the prior implicit in a denoiser. *Advances in Neural Information Processing Systems*, 34:13242–13254.

Kadkhodaie, Z. and Simoncelli, E. P. (2020). Solving linear inverse problems using the prior implicit in a denoiser. *arXiv preprint arXiv:2007.13640*.

Karras, T., Aittala, M., Aila, T., and Laine, S. (2022). Elucidating the design space of diffusion-based generative models. *Advances in neural information processing systems*, 35:26565–26577.

Kingma, D. P. and Welling, M. (2013). Auto-encoding variational bayes. *arXiv preprint arXiv:1312.6114*.

Lee, H., Lu, J., and Tan, Y. (2023). Convergence of score-based generative modeling for general data distributions. In *International Conference on Algorithmic Learning Theory*, pages 946–985. PMLR.

Li, G. and Yan, Y. (2024). Adapting to unknown low-dimensional structures in score-based diffusion models. *Advances in Neural Information Processing Systems*, 37:126297–126331.

Li, T. and He, K. (2025). Back to basics: let denoising generative models denoise. *arXiv preprint arXiv:2511.13720*.

Liang, J., Huang, Z., and Chen, Y. (2025). Low-dimensional adaptation of diffusion models: Convergence in total variation (extended abstract). In *Proceedings of Thirty Eighth Conference on Learning Theory*, volume 291 of *Proceedings of Machine Learning Research*. PMLR.

Liu, Z., Luo, P., Wang, X., and Tang, X. (2015). Deep learning face attributes in the wild. In *Proceedings of International Conference on Computer Vision (ICCV)*.

Miyasawa, K. (1961). An empirical Bayes estimator of the mean of a normal population. *Bull. Inst. Internat. Statist.*, 38:181–188.

Olshausen, B. A. and Field, D. J. (1996). Natural image statistics and efficient coding. *Network: computation in neural systems*, 7(2):333.

Pooladian, A.-A. and Niles-Weed, J. (2025). Plug-in estimation of Schrödinger bridges. *SIAM Journal on Mathematics of Data Science*, 7(3):1315–1336.

Pope, P., Zhu, C., Abdelkader, A., Goldblum, M., and Goldstein, T. (2021). The intrinsic dimension of images and its impact on learning. In *International Conference on Learning Representations*.

Potapchik, P., Azangulov, I., and Deligiannidis, G. (2024). Linear convergence of diffusion models under the manifold hypothesis. *arXiv preprint arXiv:2410.09046*.

Raphan, M. and Simoncelli, E. P. (2011). Least squares estimation without priors or supervision. *Neural Computation*, 23(2):374–420.

Ronneberger, O., Fischer, P., and Brox, T. (2015). U-net: convolutional networks for biomedical image segmentation. In *Int'l Conf Medical Image Computing and Computer-assisted Intervention*, pages 234–241. Springer.

Roweis, S. T. and Saul, L. K. (2000). Nonlinear dimensionality reduction by locally linear embedding. *Science*, 290(5500):2323–2326.

Sohl-Dickstein, J., Weiss, E., Maheswaranathan, N., and Ganguli, S. (2015). Deep unsupervised learning using nonequilibrium thermodynamics. In *International Conference on Machine Learning*, pages 2256–2265. PMLR.

Song, J., Meng, C., and Ermon, S. (2021a). Denoising diffusion implicit models. In *International Conference on Learning Representations*.

Song, Y., Sohl-Dickstein, J., Kingma, D. P., Kumar, A., Ermon, S., and Poole, B. (2021b). Score-based generative modeling through stochastic differential equations. In *International Conference on Learning Representations*.

Sun, Q., Jiang, Z., Zhao, H., and He, K. (2025). Is noise conditioning necessary for denoising generative models? In *Forty-second International Conference on Machine Learning*.

Tang, J. and Yan, Y. (2025). Adaptivity and convergence of probability flow ODEs in diffusion generative models. *arXiv preprint arXiv:2501.18863*.

Wang, R. and Du, Y. (2025). Equilibrium matching: generative modeling with implicit energy-based models. *arXiv preprint arXiv:2510.02300*.

Yu, F., Seff, A., Zhang, Y., Song, S., Funkhouser, T., and Xiao, J. (2015). LSUN: construction of a large-scale image dataset using deep learning with humans in the loop. *arXiv preprint arXiv:1506.03365*.

Zhang, K., Zuo, W., Chen, Y., Meng, D., and Zhang, L. (2017). Beyond a Gaussian denoiser: residual learning of deep CNN for image denoising. *IEEE Transactions on Image Processing*, 26(7):3142–3155.

## A Proofs for Sections 3.1 and 3.2

### A.1 Proof of Proposition 3.1

The population counterpart to (6) is

$$f^* = \operatorname{argmin}_{\substack{f: \mathbb{R}^d \rightarrow \mathbb{R}^d \\ \sigma \sim \Theta \\ z \sim \gamma}} \mathbb{E}_{\mathbf{x} \sim p_X} \|\mathbf{x} - f(\mathbf{x} + \sigma z)\|^2.$$

Let  $y := \mathbf{x} + \sigma z$ . The optimal function  $f$  of  $y$  to predict  $\mathbf{x}$  is the conditional expectation  $\mathbb{E}[\mathbf{x}|y]$ , due to orthogonality:

$$\mathbb{E}\|\mathbf{x} - f(y)\|^2 = \mathbb{E}\|\mathbf{x} - \mathbb{E}[\mathbf{x}|y]\|^2 + \mathbb{E}\|\mathbb{E}[\mathbf{x}|y] - f(y)\|^2. \quad (16)$$

On the other hand, by Bayes, we can express

$$\mathbb{E}[\mathbf{x}|y] = \int \mathbb{E}[\mathbf{x}|\sigma, y] d\mu(\sigma|y).$$

Applying Tweedie's identity (5),

$$\mathbb{E}[\mathbf{x}|y] = \int (y + \sigma^2 \nabla \log p_\sigma(y)) d\mu(\sigma|y).$$

We remark that by (16), for any estimator  $\hat{f}$ , the excess risk is

$$\begin{aligned} \mathcal{E}(\hat{f}) &:= \mathbb{E}\|\mathbf{x} - \hat{f}(y)\|^2 - \mathbb{E}\|\mathbf{x} - f^*(y)\|^2 \\ &= \mathbb{E}\|\hat{f}(y) - f^*(y)\|^2 = \int \|\hat{f} - f^*\|_{L^2(p_\sigma)}^2 d\Theta(\sigma). \end{aligned} \quad (17)$$

### A.2 Proof of Proposition 3.2

Let  $\rho_t := \text{Law}(X_t)$  and  $\tilde{\rho}_t := p_{\sigma_t} := p_X * \gamma_{\sigma_t^2}$ . We first compute directly  $\partial_t \tilde{\rho}_t$  from this definition using the fact that the Gaussian density is the solution to the heat equation:

$$\begin{aligned} \partial_t \tilde{\rho}_t(y) &= \partial_t \int \gamma_{\sigma_t^2}(y) p_X(y-x) dx \\ &= \int (\partial_t \gamma_{\sigma_t^2}(y)) p_X(y-x) dx \\ &= \int (\partial_t \sigma_t^2) (\partial_s \gamma_s|_{s=\sigma_t^2}(y)) p_X(y-x) dx \\ &= \frac{1}{2} (\partial_t \sigma_t^2) \int \Delta \gamma_{\sigma_t^2}(y) p_X(y-x) dx \\ &= \frac{1}{2} (\partial_t \sigma_t^2) \Delta_y \int \gamma_{\sigma_t^2}(y) p_X(y-x) dx \\ &= \frac{1}{2} (\partial_t \sigma_t^2) \Delta \tilde{\rho}_t(y). \end{aligned} \quad (18)$$

On the other hand, under the ideal dynamics (11), the Fokker–Planck equation reads

$$\begin{aligned} \partial_t \rho_t &= -\nabla \cdot (\rho_t \sigma_t^2 \nabla \log p_{\sigma_t}) + a_t \Delta \rho_t \\ &= -\nabla \cdot (\rho_t \sigma_t^2 \nabla \log \tilde{\rho}_t) + a_t \Delta \rho_t. \end{aligned} \quad (19)$$

Since  $\Delta\tilde{\rho}_t = \nabla \cdot (\tilde{\rho}_t \nabla \log \tilde{\rho}_t)$ , (18) shows that  $(\tilde{\rho}_t)_{t \in [0, T]}$  solves the equation (19), provided that

$$\frac{1}{2} (\partial_t \sigma_t^2) = -\sigma_t^2 + a_t. \quad (20)$$

By uniqueness of solutions to the Fokker–Planck equation, we see that with this choice of  $(\sigma_t)_{t \in [0, T]}$  and for  $\rho_0 = \tilde{\rho}_0$ , we have  $\rho_t = \tilde{\rho}_t$  for all  $t \in [0, T]$ . Solving the ODE (20) yields the claim.

### A.3 Proof of Lemma 3.3

Recall that  $\frac{1}{2} \partial_t (\sigma_t^2) = -\sigma_t^2 + a_t$ , so we want to show  $a_t \leq \sigma_t^2$  for all  $t \geq 0$ . Note that if  $a_t \leq a_0 \leq \sigma_0^2$  for all  $t \geq 0$ , then

$$\sigma_t^2 = \sigma_0^2 e^{-2t} + 2 \int_0^t a_s e^{-2(t-s)} ds \geq \sigma_0^2 e^{-2t} + a_t (1 - e^{-2t}).$$

This is lower bounded by  $a_t$  provided  $a_t \leq \sigma_0^2$ .

### A.4 Proof of Lemma 3.4

The first term in Proposition 3.2 is obviously decaying to zero, so we must show that  $2 \int_0^t a_s e^{-2(t-s)} ds \rightarrow 0$ . Since  $a_t \rightarrow 0$ , for any  $\varepsilon > 0$  there exists  $t_0$  such that  $a_t \leq \varepsilon$  for all  $t \geq t_0$ . Then, for  $t \geq t_0$ ,

$$\begin{aligned} \int_0^t 2a_s e^{-2(t-s)} ds &\leq \int_0^{t_0} (\dots) + \int_{t_0}^t (\dots) \\ &\leq a_0 (e^{-2(t-t_0)} - e^{-2t}) + \varepsilon (1 - e^{-2(t-t_0)}) \\ &\leq a_0 (e^{-2(t-t_0)} - e^{-2t}) + \varepsilon. \end{aligned}$$

We can choose  $t$  sufficiently large to make the first term at most  $\varepsilon$  as well.

## B Proofs for Sections 3.3 and 3.4

We use the following notation throughout the appendix. Let  $p_\omega := p * \mathcal{N}(0, \omega^2 I)$ . Write  $q_\omega$  for the joint distribution under which  $X \sim p_X$ ,  $Y \sim \mathcal{N}(X, \omega^2 I)$ . We also denote

$$\begin{aligned} f_\omega^\star(y) &:= \mathbb{E}_{q_\omega}[X|Y=y], \\ C_\omega(y) &:= \mathbb{E}_{q_\omega}[(X - f_\omega^\star(y))^{\otimes 2}] = \text{Cov}_{q_\omega}(X|Y=y), \\ W_\omega(y) &:= \text{Cov}_{q_\omega}(X, \|X - y\|^2|Y=y), \\ Q_\omega(x, y) &:= \langle y - x, C_\omega(y)(y - x) \rangle. \end{aligned}$$

Also, since we repeatedly encounter the quantity  $k + \log(1/\delta)$  for some  $\delta > 0$ , we abbreviate this by  $k_\delta$ .

## B.1 Bound on the cross-covariance

**Proposition B.1.** *Under (A1) and (A2), for  $X_t \sim p_{\sigma_t}$ , with high probability,*

$$\|W_\omega(X_t)\| \lesssim (\sigma_t^2 + \omega^2) (R + \sqrt{k}) k.$$

Moreover,

$$\begin{aligned} \mathbb{E} \left[ \left| \int_\sigma^{\sigma_t} \|W_\omega(X_t)\| \omega^{-3} d\omega \right|^2 d\mu(\sigma|X_t) \right] \\ \lesssim_{\log} (R^2 + k) k^2 \mathbb{E} \int (|1 - \sigma_t^2/\sigma^2|^2 + |\log(\sigma_t/\sigma)|^2) d\mu(\sigma|X_t). \end{aligned}$$

*Proof.* Recall that

$$\partial_\omega(\omega^2 \nabla \log p_\omega(y)) = \omega^{-3} W_\omega(y) := \omega^{-3} \text{Cov}_{q_\omega}(X, \|Y - X\|^2 | Y = y). \quad (21)$$

By Lemma F.4, it holds that

$$\|W_\omega(X_t)\| \lesssim (R^2 \text{tr}^2 C_\omega(X_t) + \text{tr} C_\omega(X_t) Q_\omega(X, X_t))^{1/2}. \quad (22)$$

By applying Proposition F.2 (specifically Corollary F.3), on an event  $\mathcal{G}$  of probability  $1 - \delta$ , we have that

$$\begin{aligned} \|W_\omega(X_t)\| &\lesssim ((R^2 (\sigma_t^2 + \omega^2)^2 k_\delta^2 + (\sigma_t^2 + \omega^2)^2 k_\delta^3)^{1/2} \\ &\lesssim (\sigma_t^2 + \omega^2) k_\delta (R + \sqrt{k_\delta}), \end{aligned}$$

whence (again, on  $\mathcal{G}$ )

$$\begin{aligned} \left| \int_\sigma^{\sigma_t} \|W_\omega(X_t)\| \omega^{-3} d\omega \right|^2 &\lesssim k_\delta^2 (R^2 + k_\delta) \left| \int_\sigma^{\sigma_t} \sigma_t^2 \omega^{-3} d\omega + \int_\sigma^{\sigma_t} \omega^{-1} d\omega \right|^2 \\ &\lesssim k_\delta^2 (R^2 + k_\delta) \left( |1 - \sigma_t^2/\sigma^2|^2 + |\log(\sigma_t/\sigma)|^2 \right). \end{aligned}$$

On the bad event, (22) implies

$$\|W_\omega(X_t)\| \lesssim R^3 + R^2 \|X_t - X\|.$$

Hence,

$$\begin{aligned} \mathbb{E} \left[ \int \left| \int_\sigma^{\sigma_t} \|W_\omega(X_t)\| \omega^{-3} d\omega \right|^2 d\mu(\sigma|X_t) \mathbf{1}_{\mathcal{G}^c} \right] \\ &\lesssim \mathbb{E} \left[ (R^6 + R^4 \|X_t - X\|^2) \int \left| \int_\sigma^{\sigma_t} \omega^{-3} d\omega \right|^2 d\mu(\sigma|X_t) \mathbf{1}_{\mathcal{G}^c} \right] \\ &\lesssim \mathbb{E} \left[ \frac{R^6 + R^4 \|X_t - X\|^2}{\sigma_T^4} \mathbf{1}_{\mathcal{G}^c} \right] \\ &\lesssim \sqrt{\mathbb{E} \left[ \frac{R^{12} + R^8 \|X_t - X\|^4}{\sigma_T^8} \right] \mathbb{P}(\mathcal{G}^c)} \\ &\lesssim \frac{R^6 + \sigma_0^4 R^8 d^2}{\sigma_T^8} \delta^{1/2}. \end{aligned}$$

This term is negligible by choosing  $\delta$  sufficiently small.  $\square$

## B.2 Proof of Lemma 3.7

The change-of-variables formula is straightforward as  $|\frac{d\sigma}{d\lambda}| = \frac{1}{2}\lambda^{-3/2}$ . For the next part, we write

$$\ell(\lambda|y) = -\log \nu(\lambda|y) = -\frac{d-\alpha}{2} \log \lambda - \log \mathbb{E}_{X \sim p_X} \left[ \exp \left( -\frac{\lambda}{2} \|X - y\| \right) \right] + c,$$

where  $c > 0$  is an absolute constant. We compute via chain rule

$$\ell'(\lambda|y) = -\frac{d-\alpha}{2\lambda} + \frac{1}{2} \mathbb{E}_{q_\lambda} [\|X - Y\|^2 | Y = y],$$

where  $q_\lambda(x|y) \propto \exp(-\frac{\lambda}{2}\|x - y\|^2)p_X(x)$ , with  $\partial_\lambda q_\lambda(x|y) = -\frac{1}{2}\|x - y\|^2 q_\lambda$ . The second derivative is similar:

$$\ell''(\lambda|y) = \frac{d-\alpha}{2\lambda^2} - \frac{1}{4} \text{Var}_{q_\lambda} [\|X - Y\|^2 | Y = y].$$

## B.3 Proof of Proposition 3.8

**Claim 1.**  $\nu(\cdot|X_t)$  concentrates around  $\lambda_t$  with high probability.

*Proof of Claim 1.* By Proposition F.2, with probability at least  $1 - \delta$ ,

$$\begin{aligned} \ell'(\lambda|X_t) &= -\frac{d+\alpha}{\lambda} + \mathbb{E}_{q_\lambda} [\|X - Y\|^2 | Y = X_t] \\ &= -\frac{d \pm O(k_\delta)}{\lambda} + \frac{d \pm O(\sqrt{d \log(1/\delta)} + k_\delta)}{\lambda_t}. \end{aligned}$$

Define the error term

$$E = \sqrt{d \log(1/\delta)} + k_\delta.$$

Note that for  $\lambda > \lambda_t$ ,

$$\ell'(\lambda|X_t) \geq \frac{d}{\lambda_t} \left[ 1 - \frac{\lambda_t}{\lambda} - \frac{O(E)}{d} \right] \gtrsim \begin{cases} d(\lambda - \lambda_t)/\lambda_t^2, & \lambda_t E/d \ll \lambda - \lambda_t \leq \lambda_t, \\ d/\lambda_t, & \lambda - \lambda_t \geq \lambda_t, \end{cases}$$

where we require that  $E/d \ll 1$ , i.e.,  $d \gg_{\log} k$ . Therefore, for  $a \gg \lambda_t E/d$ , we can integrate to find that

$$\begin{aligned} \int_{\lambda_t+a}^{\infty} d\nu(\lambda|X_t) &\leq \int_{\lambda_t+a}^{2\lambda_t} \nu(\lambda_t|X_t) \exp(-\Omega(d(\lambda - \lambda_t)^2/\lambda_t^2)) d\lambda \\ &\quad + \int_{2\lambda_t}^{\lambda_{\max}} \nu(\lambda_t|X_t) \exp(-\Omega(d)) d\lambda \\ &\lesssim \left[ \frac{\lambda_t}{ad^{1/2}} \exp(-\Omega(da^2/\lambda_t^2)) + \lambda_{\max} \exp(-\Omega(d)) \right] \nu(\lambda_t|X_t). \end{aligned}$$

On the other hand, for  $|\lambda - \lambda_t| \ll \lambda_t E/d$ , one has  $|\ell'(\lambda|X_t)| \lesssim E/\lambda_t$ . Hence,

$$\begin{aligned} \nu(\lambda_t|X_t) &\lesssim \frac{d}{\lambda_t E} \int_{|\lambda - \lambda_t| \leq c\lambda_t E/d} \nu(\lambda_t|X_t) d\lambda \\ &\lesssim \frac{d}{\lambda_t E} \int_{|\lambda - \lambda_t| \leq c\lambda_t E/d} \nu(\lambda|X_t) \exp(O(E(\lambda - \lambda_t)/\lambda_t)) d\lambda \\ &\lesssim \frac{d}{E^2} \exp(O(E^2/d)), \end{aligned}$$

and thus

$$\int_{\lambda_t+a}^{\infty} d\nu(\lambda|X_t) \lesssim \frac{\lambda_t d^{1/2}}{a} \exp(O(\mathsf{E}^2/d) - \Omega(da^2/\lambda_t^2)) + \frac{\lambda_{\max} d}{\mathsf{E}^2} \exp(O(\mathsf{E}^2/d) - \Omega(d)).$$

If  $d \gg k$  and we choose  $a \gg \lambda_t \mathsf{E}/d$  up to logarithmic factors, this shows that with very high probability under  $\nu(\cdot | X_t)$ ,

$$\lambda \leq \lambda_t \left[ 1 + \tilde{O}\left(\frac{1}{\sqrt{d}} + \frac{k}{d}\right) \right].$$

A similar argument gives the corresponding lower bound.  $\square$

**Claim 2.**

$$\mathbb{E} \left[ \int (|\log(\lambda_t/\lambda)|^2 + |1 - \lambda_t/\lambda|^2) d\nu(\lambda|X_t) \right] \lesssim_{\log} \frac{1}{d} + \frac{k^2}{d^2}.$$

*Proof of Claim 2.* Let  $\mathcal{H}$  be the event of high probability from Claim 1. On this event,  $\lambda \in [c\lambda_t, C\lambda_t]$  for universal constants  $c, C > 0$ , provided that  $d \gg_{\log} k$ . We can break up the term of interest into

$$\mathbb{E} \left[ \int (|\log(\lambda_t/\lambda)|^2 + |1 - \lambda_t/\lambda|^2) d\nu(\lambda|X_t) \mathbf{1}_{\mathcal{H}} \right] + \mathbb{E} \left[ \int (|\log(\lambda_t/\lambda)|^2 + |1 - \lambda_t/\lambda|^2) d\nu(\lambda|X_t) \mathbf{1}_{\mathcal{H}^c} \right].$$

Focusing on the good event, since  $\lambda$  is within a constant factor of  $\lambda_t$ , the first term above is bounded by

$$\begin{aligned} \mathbb{E} \left[ \int (|\log(\lambda_t/\lambda)|^2 + |1 - \lambda_t/\lambda|^2) d\nu(\lambda|X_t) \mathbf{1}_{\mathcal{H}} \right] &\lesssim \frac{1}{\lambda_t^2} \mathbb{E} \int |\lambda_t - \lambda|^2 d\nu(\lambda | X_t) \\ &\lesssim_{\log} \frac{1}{d} + \frac{k^2}{d^2}. \end{aligned}$$

For the second term, we can uniformly bound the integrand, yielding

$$(\log(\lambda_{\max}/\lambda_{\min}) + |\lambda_{\max}/\lambda_{\min} - 1|)^2 \mathbb{P}(\mathcal{H}^c).$$

Now choose the probability  $\delta$  of the bad event to be extremely small so that the term on the bad event is negligible. This leads to the claimed bound.  $\square$

These two claims establish Proposition 3.8.

## B.4 Proof of Theorem 3.6

Recall the KL error decomposition. For the first term, we use the standard fact

$$\text{KL}(p_{\sigma_0} \| \hat{p}_0) = \text{KL}(p_X * \gamma_{\sigma_0^2} \| \gamma_{\sigma_0}^2) \leq \frac{1}{2\sigma_0^2} W_2^2(p_X, \delta_0) = \frac{\mathbb{E}_{X \sim p_X} [\|X\|^2]}{2\sigma_0^2} \leq \frac{R^2}{2\sigma_0^2}.$$

The second term is due to the definition of  $\varepsilon_{\text{BD}}^2$ , and the third term follows from the analysis of Section 3.4.

## C Proofs for Section 3.5

### C.1 Exponential Euler discretization

In order to establish discretization guarantees which only scale with the intrinsic dimension, we use the exponential Euler discretization: for fixed step size  $h > 0$ , the algorithm follows

$$dY_t = (\hat{f}(Y_{t-}) - Y_t) dt + \sqrt{2a_t} dB_t, \quad (23)$$

where  $t_- := \lfloor t/h \rfloor h$ . In other words, we freeze the non-linear term  $\hat{f}$  and exactly integrate the rest, including the linear term. Some intuition for this can be seen as follows: if, instead of  $\hat{f}$ , we had  $f_{\sigma_t}^*$ , then the Jacobian of the drift is  $C_{\sigma_t}/\sigma_t^2 - I$ . Generally, discretization error bounds rely on Lipschitz bounds on the drift, i.e., bounds on the operator norm of this Jacobian. However, among the two terms in the Jacobian, only the first—a conditional covariance matrix—is expected to be controlled in terms of the intrinsic dimension. This suggests that to avoid dependence on the ambient dimension, we should exactly integrate the  $-Y_t$  term.

### C.2 Proof of Theorem 3.9

Recall that  $f_{\sigma_t}^* = \text{id} + \sigma_t^2 \nabla \log p_{\sigma_t}$ . To control the discretization error, we first need an Itô calculation.

**Lemma C.1.** *Let  $(\sigma_t)_{t \geq 0}$  be as in Proposition 3.2. Then*

$$\partial_t f_{\sigma_t}^*(y) = \dot{\sigma}_t \partial_\omega (\omega^2 \nabla \log p_\omega(y))|_{\omega=\sigma_t} = \left( \frac{a_t}{\sigma_t^4} - \frac{1}{\sigma_t^2} \right) W_{\sigma_t}(y).$$

*Proof.* Follows from the chain rule, (21), and the final expression for  $\dot{\sigma}_t$  from (20).  $\square$

**Proposition C.2.** *For  $X_t$  following (11), it holds that*

$$df_{\sigma_t}^*(X_t) = \left\{ \frac{2a_t - \sigma_t^2}{\sigma_t^4} \left( W_{\sigma_t}(X_t) - C_{\sigma_t}(X_t) f_{\sigma_t}^*(X_t) \right) \right\} dt + \sqrt{2a_t} \sigma_t^{-2} C_{\sigma_t}(X_t) dB_t.$$

*Proof.* Writing out Itô's lemma,

$$df_{\sigma_t}^*(X_t) = (\partial_t f_{\sigma_t}^*)(X_t) dt + \langle \nabla f_{\sigma_t}^*(X_t), dX_t \rangle + \frac{1}{2} \langle dX_t, \nabla^2 f_{\sigma_t}^*(X_t) dX_t \rangle$$

we see that the only terms that remain are

$$\begin{aligned} df_{\sigma_t}^*(X_t) &= [(\partial_t f_{\sigma_t}^*)(X_t) + \nabla f_{\sigma_t}^*(X_t)(f_{\sigma_t}^*(X_t) - X_t) + a_t \Delta f_{\sigma_t}^*(X_t)] dt \\ &\quad + \sqrt{2a_t} \nabla f_{\sigma_t}^*(X_t) dB_t. \end{aligned}$$

From Lemma C.1 we have that

$$\partial_t f_{\sigma_t}^*(y) = \frac{a_t - \sigma_t^2}{\sigma_t^4} W_{\sigma_t}(y)$$

and by Tweedie's formula (recall Lemma F.1)

$$a_t \Delta f_{\sigma_t}^* = a_t \sigma_t^2 \Delta \nabla \log p_{\sigma_t} = a_t \sigma_t^2 \nabla \Delta \log p_{\sigma_t} = a_t \sigma_t^{-2} \nabla \operatorname{tr} C_{\sigma_t},$$

where the identity matrix drops due to the additional gradient. Finally, note that

$$\nabla f_{\sigma_t}^*(y)(f_{\sigma_t}^*(y) - y) = \sigma_t^{-2} C_{\sigma_t}(y)(f_{\sigma_t}^*(y) - y).$$

Collecting these three terms and invoking the last result in Lemma F.1, we obtain

$$\begin{aligned} & ((\partial_t f_{\sigma_t}^*) + \nabla f_{\sigma_t}^*(f_{\sigma_t}^* - \operatorname{id}) + a_t \Delta f_{\sigma_t}^*)(y) \\ &= \frac{a_t - \sigma_t^2}{\sigma_t^4} W_{\sigma_t}(y) + a_t \sigma_t^{-2} (\nabla \operatorname{tr} C_{\sigma_t}(y)) + \sigma_t^{-2} C_{\sigma_t}(y)(f_{\sigma_t}^*(y) - y) \\ &= \left( \frac{a_t - \sigma_t^2}{\sigma_t^4} \right) W_{\sigma_t}(y) + \left( \frac{a_t}{\sigma_t^4} W_{\sigma_t}(y) - \frac{2a_t}{\sigma_t^4} C_{\sigma_t}(y)(f_{\sigma_t}^*(y) - y) \right) \\ &\quad + \sigma_t^{-2} C_{\sigma_t}(y)(f_{\sigma_t}^*(y) - y) \\ &= \frac{2a_t - \sigma_t^2}{\sigma_t^4} \left( W_{\sigma_t}(y) - C_{\sigma_t}(y)(f_{\sigma_t}^*(y) - y) \right). \end{aligned}$$

□

We now present the main computations from Section 3.5. Applying Girsanov's theorem to the ideal process (11), denoted  $\mathbb{P}$ , and the exponential Euler discretization (23), denoted  $\widehat{\mathbb{P}}$ , the error becomes

$$\begin{aligned} \operatorname{KL}(\mathbb{P} \parallel \widehat{\mathbb{P}}) &\lesssim \operatorname{KL}(p_0 \parallel \widehat{p}_0) + \mathbb{E} \int_0^T \frac{1}{a_t} \|\widehat{f}_\theta(X_{t-}) - f_{\sigma_t}^*(X_t)\|^2 dt \\ &\lesssim \operatorname{KL}(p_0 \parallel \widehat{p}_0) + \mathbb{E} \int_0^T \frac{1}{a_t} (\|\widehat{f}_\theta(X_{t-}) - f^*(X_{t-})\|^2 + \|f^*(X_{t-}) - f_{\sigma_{t-}}^*(X_{t-})\|^2 + \|f_{\sigma_{t-}}^*(X_{t-}) - f_{\sigma_t}^*(X_t)\|^2) dt \\ &\lesssim \operatorname{KL}(p_0 \parallel \widehat{p}_0) + \tilde{\varepsilon}_{\text{BD}}^2 + \mathbb{E} \int_0^T \frac{1}{a_t} \|f^*(X_{t-}) - f_{\sigma_{t-}}^*(X_{t-})\|^2 dt \\ &\quad + \mathbb{E} \int_0^T \frac{1}{a_t} \|f_{\sigma_{t-}}^*(X_{t-}) - f_{\sigma_t}^*(X_t)\|^2 dt \\ &\lesssim_{\log} \operatorname{KL}(p_0 \parallel \widehat{p}_0) + \tilde{\varepsilon}_{\text{BD}}^2 + \frac{(R^2 + \kappa) \kappa^2}{d} A_T \int_0^T \frac{1}{a_t} \mathbb{E} \|f_{\sigma_{t-}}^*(X_{t-}) - f_{\sigma_t}^*(X_t)\|^2 dt \end{aligned} \tag{24}$$

where we used the result from Theorem 3.6 in the last line.

For the last term, we have by Proposition C.2 and the Itô isometry,

$$\begin{aligned} & \mathbb{E} \|f_{\sigma_{t-}}^*(X_{t-}) - f_{\sigma_t}^*(X_t)\|^2 \\ &= \mathbb{E} \left\| \int_{t-}^t \left\{ \frac{2a_s - \sigma_s^2}{\sigma_s^4} \left( W_{\sigma_s}(X_s) - C_{\sigma_s}(X_s) f_{\sigma_{t-}}^*(X_s) \right) \right\} ds + \sqrt{2a_s} \sigma_s^{-2} C_{\sigma_s}(X_s) dB_s \right\|^2 \\ &\lesssim h \int_{t-}^t \left( \frac{2a_s - \sigma_s^2}{\sigma_s^4} \right)^2 \mathbb{E} \|W_{\sigma_s}(X_s) - C_{\sigma_s}(X_s) f_{\sigma_t}^*(X_s)\|^2 ds \\ &\quad + \int_{t-}^t a_s \sigma_s^{-4} \mathbb{E} \|C_{\sigma_s}(X_s)\|_{\text{F}}^2 ds. \end{aligned}$$

From Proposition B.1 and Corollary F.3, we can bound w.h.p.

$$\begin{aligned}\mathbb{E}\|C_{\sigma_s}(X_s)\|_{\text{F}}^2 &\leq \mathbb{E} \text{tr}^2 C_{\sigma_s}(X_s) \lesssim_{\log} \sigma_s^4 \mathbf{k}^2, \\ \mathbb{E}\|W_{\sigma_s}(X_s)\|^2 &\lesssim_{\log} \sigma_s^4 \mathbf{k}^3, \\ \mathbb{E}\|C_{\sigma_s}(X_s)f_s(X_s)\|^2 &\lesssim_{\log} R^2 \sigma_s^4 \mathbf{k}^2,\end{aligned}$$

which gives

$$\mathbb{E}\|f_{\sigma_{t_-}}^*(X_{t_-}) - f_{\sigma_t}^*(X_t)\|^2 \lesssim_{\log} h R^2 \mathbf{k}^3 \int_{t_-}^t \left(\frac{2a_s - \sigma_s^2}{\sigma_s^4}\right)^2 \sigma_s^4 \, ds + \mathbf{k}^2 \int_{t_-}^t a_s \, ds.$$

Note that if we want  $\partial_t(\sigma_t^2) = -2\sigma_t^2 + 2a_t$  to be negative, then we require  $a_t \leq \sigma_t^2$ . Therefore, assuming that this holds,  $-\sigma_s^2 \leq 2a_s - \sigma_s^2 \leq \sigma_s^2$ . So, we can bound the above by

$$\mathbb{E}\|f_{\sigma_{t_-}}^*(X_{t_-}) - f_{\sigma_t}^*(X_t)\|^2 \lesssim_{\log} h^2 R^2 \mathbf{k}^3 + \mathbf{k}^2 \int_{t_-}^t a_s \, ds$$

Note, however, that the first term vanishes entirely when  $a_t = \sigma_t^2/2$  for all  $t$ !

Let us assume that the noise schedule is regularly varying, in the sense that  $t \mapsto \log a_t$  is  $\ell$ -Lipschitz and that the step size is always at most  $1/\ell$ . This ensures that on each interval  $[t_-, t]$ , the values of  $a$  only differ by a universal constant. In particular, for the special family of noise schedules, we have  $\log a_t = -2(1-\mathbf{a})t + \text{const.}$ , so this holds with  $\ell = 2(1-\mathbf{a})$ .

This allows us to simplify the above statement into

$$\mathbb{E}\|f_{\sigma_{t_-}}^*(X_{t_-}) - f_{\sigma_t}^*(X_t)\|^2 \lesssim_{\log} h^2 R^2 \mathbf{k}^3 + h a_t \mathbf{k}^2.$$

Integrating, we find that

$$\text{Disc}(h) \lesssim_{\log} R^2 \mathbf{k}^3 h^2 \int_0^T \frac{1}{a_t} \, dt + \mathbf{k}^2 h T = R^2 \mathbf{k}^3 h^2 A_T + \mathbf{k}^2 h T.$$

Next, let us specialize further to the class of noise schedules with  $a_t = \mathbf{a}\sigma_t^2$  for some  $\mathbf{a} \in (0, 1)$ . In this case,

$$\begin{aligned}A_T &= \frac{1}{\mathbf{a}\sigma_0^2} \int_0^T \exp(2(1-\mathbf{a})t) \, dt = \frac{\exp(2(1-\mathbf{a})T) - 1}{2\mathbf{a}(1-\mathbf{a})\sigma_0^2} = \frac{1}{2\mathbf{a}(1-\mathbf{a})} (1/\sigma_T^2 - 1/\sigma_0^2) \\ &\leq \frac{1}{2\mathbf{a}(1-\mathbf{a})\sigma_T^2}.\end{aligned}\tag{25}$$

With this, we have our final bound

$$\text{Disc}(h) \lesssim_{\log} \frac{R^2 \mathbf{k}^3 h^2}{\mathbf{a}(1-\mathbf{a})\sigma_T^2} \mathbf{1}_{\mathbf{a} \neq 1/2} + \mathbf{k}^2 h \frac{\log(\sigma_0^2/\sigma_T^2)}{2(1-\mathbf{a})},$$

where we used the fact that one of the error terms vanishes exactly when  $\mathbf{a} = 1/2$ .

## D Proofs for Section 3.6

### D.1 Early stopping in the perceptual metric

**Lemma D.1.** *It holds that  $W_{1,\mathcal{X}}(p_X, p_\sigma) \lesssim \sigma\sqrt{k}$ , where*

$$W_{1,\mathcal{X}}(\mu, \nu) := \sup\{\mathbb{E}_\mu(f \circ \Pi_{\mathcal{X}}) - \mathbb{E}_\nu(f \circ \Pi_{\mathcal{X}}) : \|f\|_{\text{Lip}} \leq 1\}$$

and  $\Pi_{\mathcal{X}}$  is the projection onto  $\mathcal{X} = \text{supp}(p_X)$ .

*Remark D.2.* Since  $\mathcal{X}$  is compact, it is possible to take  $\Pi_{\mathcal{X}}$  measurable.

*Proof of Lemma D.1.* First, note that a coupling argument shows that the quantity of interest is bounded by  $\mathbb{E}\|X - \Pi_{\mathcal{X}}(X + V)\|$  where  $V \sim \mathcal{N}(0, \sigma^2 I)$ . Let  $x_1, \dots, x_N$  be the centers of a  $r_0$ -covering of  $\mathcal{X}$ . Then, by Claim 1 in Proposition F.2, we know that with probability at least  $1 - \delta$ , for all  $x, x' \in \mathcal{X}$ ,

$$|\langle V, x - x' \rangle| \lesssim \sigma\sqrt{k_\delta} \|x - x'\| + r_0\sigma\sqrt{d + \log(1/\delta)}.$$

Note that if  $x$  is the closest center in the covering to the point  $X$ , then

$$\begin{aligned} \|X + V - x\|^2 &= \|V\|^2 + \|X - x\|^2 + 2\langle V, X - x \rangle \\ &\leq \|V\|^2 + O(r_0^2 + r_0\sigma\sqrt{d + \log(1/\delta)}). \end{aligned}$$

On the other hand, if  $X' := \Pi_S(X + V)$ ,

$$\begin{aligned} \|X + V - X'\|^2 &= \|V\|^2 + \|X - X'\|^2 + 2\langle V, X - X' \rangle \\ &\geq \|V\|^2 + \|X - X'\|^2 - O(\sigma\sqrt{k_\delta} \|X - X'\| + r_0\sigma\sqrt{d + \log(1/\delta)}). \end{aligned}$$

By definition of  $X'$ ,  $\|X + V - X'\| \leq \|X + V - x\|$ . Hence,

$$\|X - X'\|^2 \lesssim \sigma\sqrt{k_\delta} \|X - X'\| + r_0^2 + r_0\sigma\sqrt{d + \log(1/\delta)},$$

and by Young's inequality, this can be rearranged to yield

$$\|X - X'\|^2 \lesssim \sigma^2 k_\delta + r_0^2 + r_0\sigma\sqrt{d + \log(1/\delta)}.$$

Since  $r_0 \leq \sigma/\sqrt{d}$ , this readily yields

$$\|X - X'\|^2 \lesssim \sigma^2(k + \log(1/\delta)).$$

By integrating this tail bound,  $\mathbb{E}\|X - \Pi_S(X + V)\| = \mathbb{E}\|X - X'\| \lesssim \sigma\sqrt{k}$ .  $\square$

### D.2 Proof of Corollary 3.10

By (24), (25), and Theorem 3.9,

$$\text{KL}(p_{\sigma_T} \| \hat{p}_T) \lesssim_{\log} \frac{R^2}{\sigma_0^2} + \tilde{\varepsilon}_{\text{BD}}^2 + \frac{(R^2 + k)k^2}{d\sigma_T^2} + k^2h.$$

We choose  $\sigma_0 \asymp R/\varepsilon$ ,  $h \asymp_{\log} \varepsilon^2/k^2$ , and  $d \gg_{\log} (R^2 + k)k^2/(\sigma_T^2\varepsilon^2)$  to ensure that  $\text{KL}(p_{\sigma_T} \parallel \hat{p}_T) \lesssim \tilde{\varepsilon}_{\text{BD}}^2 + \varepsilon^2$ . By Pinsker's inequality, and noting that the total variation distance clearly upper bounds  $D_{\mathcal{X}}$ , it implies  $D_{\mathcal{X}}(\hat{p}_T, p_{\sigma_T}) \lesssim \varepsilon_{\text{BD}} + \varepsilon$ .

Then, Lemma D.1 implies that with  $\sigma_T \asymp \varepsilon/\sqrt{k}$ , we have  $D_{\mathcal{X}}(p_{\sigma_T}, p_X) \leq \varepsilon$ . By the triangle inequality (which follows from the variational definition), it implies  $D_{\mathcal{X}}(\hat{p}_T, p_X) \lesssim \tilde{\varepsilon}_{\text{BD}} + \varepsilon$ .

The requirement on  $d$  becomes  $d \gg_{\log} (R^2 + k)k^3/\varepsilon^4$ . As for the number of iterations, note that

$$N = \frac{T}{h} = \frac{1}{h} \log(\sigma_0/\sigma_T) \asymp_{\log} \frac{k^2}{\varepsilon^2}.$$

## E Proofs for Section 3.7

### E.1 Proof of Theorem 3.12

By the definition of  $\varepsilon_{\text{BD}}^2$  and from (17),

$$\varepsilon_{\text{BD}}^2 = \int_0^T \frac{1}{a_t} \|\hat{f}_\theta - f^*\|_{L^2(p_{\sigma_t})}^2 dt, \quad \mathcal{E}(\hat{f}_\theta) = \int \|\hat{f}_\theta - f^*\|_{L^2(p_\sigma)} d\Theta(\sigma).$$

Let us switch notation to  $a(t) := a_t$ ,  $\sigma(t) := \sigma_t$ , and we perform the change of variables  $\omega = \sigma(t)$  so that  $d\omega = \dot{\sigma}(t) dt$ . Then, for  $\varepsilon(\sigma) := \|\hat{f}_\theta - f^*\|_{L^2(p_\sigma)}$ , the integral on the left can be written

$$\varepsilon_{\text{BD}}^2 = \int_0^T \frac{\varepsilon(\sigma(t))^2}{a(t)} \frac{1}{\dot{\sigma}(t)} \dot{\sigma}(t) dt = \int_{\sigma^{-1}(0)}^{\sigma^{-1}(T)} \frac{\varepsilon(\omega)^2}{a(\sigma^{-1}(\omega)) \dot{\sigma}(\sigma^{-1}(\omega))} d\omega.$$

Next, we specialize to the noise schedule with  $a(t) = a\sigma(t)^2$ ,  $\dot{\sigma}(t) = -(1-a)\sigma(t)$ . This yields

$$\begin{aligned} \varepsilon_{\text{BD}}^2 &= - \int_{\sigma^{-1}(0)}^{\sigma^{-1}(T)} \frac{\varepsilon(\omega)^2}{a\omega^2(1-a)\omega} d\omega = \int_{\sigma^{-1}(T)}^{\sigma^{-1}(0)} \frac{1}{a(1-a)\omega^3\Theta(\omega)} \varepsilon(\omega)^2 d\Theta(\omega) \\ &\leq \left( \max_{\omega \in [\sigma^{-1}(T), \sigma^{-1}(0)]} \frac{1}{a(1-a)\omega^3\Theta(\omega)} \right) \mathcal{E}(\hat{f}_\theta). \end{aligned}$$

When  $\Theta(\omega) \propto \omega^{-3}$  on  $[\sigma_T, \sigma_0]$ , where  $\sigma_T = \sigma_T$  and  $\sigma_0 = \sigma_0$ , then  $\varepsilon_{\text{BD}}^2 \propto \mathcal{E}(\hat{f}_\theta)$ .

## F Technical results

### F.1 Calculations based on Tweedie's formula

**Lemma F.1.** *The following hold*

$$\omega^2 \nabla \log p_\omega(y) = f_\omega^*(y) - y, \tag{26}$$

$$\omega^2 \nabla^2 \log p_\omega(y) = \omega^{-2} C_\omega(y) - I, \tag{27}$$

$$\omega^2 \nabla \text{tr } C_\omega(y) = W_\omega(y) - 2C_\omega(y)(f_\omega^*(y) - y). \tag{28}$$

*Proof.* We only prove the third inequality, as it is the least standard. Also, we will temporarily drop the conditioning variable and write  $\mathbb{E}_\omega$  as shorthand for  $\mathbb{E}_{q_\omega(\cdot|y)}$ .

We first notice that

$$\mathbb{E}_\omega \|X - y\|^2 = \text{Tr}(C_\omega(y)) + \|f_\omega^*(y) - y\|^2.$$

Thus the expression for  $W_\omega(y)$  simplifies to

$$W_\omega(y) = \mathbb{E}_\omega[(X - f_\omega^*(y))\|X - f_\omega^*(y)\|^2] + 2C_\omega(y)(f_\omega^*(y) - y).$$

We now want to show

$$\nabla \text{tr } C_\omega(y) = \omega^{-2} \mathbb{E}_\omega[(X - f_\omega^*(y))\|X - f_\omega^*(y)\|^2].$$

To this end, we compute (here note the gradients are with respect to  $y$ )

$$\begin{aligned} \nabla_y \text{tr } C_\omega(y) &= \nabla \int \|X - f_\omega^*(y)\|^2 q_\omega(x|y) \\ &= \int \nabla_y f_\omega^*(y)(x - f_\omega^*(y)) q_\omega(x|y) + \int \|x - f_\omega^*(y)\|^2 (\nabla_y \log q_\omega(x|y)) q_\omega(x|y) \\ &= \int \|x - f_\omega^*(y)\|^2 (\nabla_y \log q_\omega(x|y)) q_\omega(x|y). \end{aligned}$$

And finally we complete the claim by computing the following

$$\begin{aligned} \nabla_y \log q_\omega(x|y) &= \nabla_y \log p(x) - \frac{1}{2\omega^2} \nabla_y \|x - y\|^2 - \nabla \log Z_\omega(y) \\ &= 0 + \frac{1}{\omega^2}(x - y) - \nabla_y \log \int p(x) \exp\left(-\frac{1}{2\omega^2}\|x - y\|^2\right) dx \\ &= +\frac{1}{\omega^2}(x - y) - \int \left(\frac{\omega^{-2}(x - y)p(x) \exp\left(-\frac{1}{2\omega^2}\|x - y\|^2\right)}{Z_\omega(y)}\right) dx \\ &= \frac{1}{\omega^2}(x - y - f_\omega^*(y) + y) = \frac{1}{\omega^2}(x - f_\omega^*(y)). \end{aligned}$$

where  $Z_\omega(y)$  is the normalizing constant of  $q_\omega(\cdot|y)$ ; this completes the claim.  $\square$

## F.2 Tools for proving the main results

Letting  $N_X(r) = N(\mathcal{X}; r, \|\cdot\|)$  be the covering number of  $\mathcal{X}$  under the Euclidean norm, recall that

$$k = 1 + \log N_X(\sigma_T^2 / (\sigma_0 \sqrt{d})).$$

We also define

$$H(x) := \sigma^{-2} \text{Cov}(X_0 \mid X = x),$$

under the joint distribution of  $X_0 \sim p_X$ ,  $X \sim \mathcal{N}(X_0, \sigma^2 I)$ . The following proposition is adapted from [Chen et al. \(2026, Proposition E.7\)](#). To make the presentation more self-contained and because we changed the statement slightly, we provide a proof here.

**Proposition F.2.** For  $\tilde{\sigma} \geq 0$ , we write  $\mathbb{P}_{\tilde{\sigma}}(\cdot)$  to be the probability of  $(\bar{x}, V)$  under  $\bar{x} \sim p_X, V \sim \mathcal{N}(0, \tilde{\sigma}^2 I)$ .

For any  $\sigma \geq \sigma_T$ , for any  $\delta \in (0, 1)$ , it holds that

$$\mathbb{P}_{\tilde{\sigma}}(\sigma^2 \operatorname{tr}(H(\bar{x} + V)) \geq C(\tilde{\sigma}^2 + \sigma^2)(k + \log(1/\delta))) \leq \delta, \quad (29)$$

$$\mathbb{P}_{\tilde{\sigma}}(\|V\|_{H(\bar{x} + V)} \geq C(\tilde{\sigma} + \sigma)(k + \log(1/\delta))) \leq \delta. \quad (30)$$

Moreover,

$$|\mathbb{E}_{\sigma}[\|X - X_0\|^2 | X] - \tilde{\sigma}^2 d| \lesssim \tilde{\sigma}^2 \sqrt{d \log(1/\delta)} + (\tilde{\sigma}^2 + \sigma^2)(k + \log(1/\delta)) \quad (31)$$

holds with probability at least  $1 - \delta$ .

As a corollary, we obtain the following inequalities.

**Corollary F.3.** If  $X_t \sim p_{\sigma_t}$  and  $\sigma \geq \sigma_T$ , then with probability at least  $1 - \delta$ ,

$$\begin{aligned} \operatorname{tr} C_{\sigma}(X_t) &\lesssim (\sigma_t^2 + \sigma^2)(k + \log(1/\delta)), \\ Q_{\sigma}(X, X_t) &\lesssim (\sigma_t^2 + \sigma^2)(k + \log(1/\delta))^2. \end{aligned} \quad (32)$$

*Proof of Proposition F.2.* Let  $r = \frac{\sigma_T^2}{\tilde{\sigma}\sqrt{d}}$ , and fix an  $r$ -covering of  $\mathcal{X}$ , denoted  $\mathcal{X} \subseteq \bigcup_{i=1}^N B_i$ , where  $N = N_X(r)$  and  $B_i = B(z_i, r)$  from  $i = 1, \dots, N$ . Additionally, let  $\mathcal{I} = \{i \in [N] : p_X(B_i) \geq \alpha\}$  for some  $\alpha > 0$  to be chosen later, and let  $\mathcal{X}_+ = \bigcup_{i \in \mathcal{I}} B_i$ .

**Claim 1.** Define  $M_1 = \tilde{\sigma}(\sqrt{d} + \sqrt{\log(2/\delta)})$ ,  $M_2 = 8\tilde{\sigma}\sqrt{\log(2N/\delta)}$ ,

$$\mathcal{V} := \{V : \|V\| \leq M_1, |\langle V, x - x' \rangle| \leq M_2 \|x - x'\| + 2r(M_1 + M_2), \forall x, x' \in \mathcal{X}\}.$$

Then for any  $\tilde{\sigma} \in [0, 2\sigma]$ , it holds that  $\mathbb{P}_{V \sim \mathcal{N}(0, \tilde{\sigma}^2 I)}(V \notin \mathcal{V}) \leq \delta$ .

**Proof of Claim 1.** We denote  $\mathbb{Q}(\cdot) := \mathbb{P}_{V \sim \mathcal{N}(0, \tilde{\sigma}^2 I)}(\cdot)$ . By Gaussian concentration, it is clear that for  $t \geq 0$ ,

$$\mathbb{Q}(\|V\| \geq \tilde{\sigma}(\sqrt{d} + 2\sqrt{t})) \leq e^{-t}.$$

Further, for any  $i, j \in [N]$ , it holds that  $\mathbb{Q}(|\langle V, z_i - z_j \rangle| \leq \tilde{\sigma} \|z_i - z_j\| \sqrt{2t}) \leq 2e^{-t}$  for  $t \geq 0$ . Hence, by union bound, we can show that  $\mathbb{Q}(V \notin \mathcal{V}_0) \leq \delta$ , where

$$\mathcal{V}_0 = \{V : \|V\| \leq M_1, |\langle V, z_i - z_j \rangle| \leq M_2 \|z_i - z_j\|, \forall i, j \in [N]\}.$$

Note that for any  $V \in \mathcal{V}_0$ , it is clear that for any  $i, j \in [N]$ ,  $x \in B_i, x' \in B_j$ , we can bound

$$\begin{aligned} |\langle V, x - x' \rangle| &\leq |\langle V, z_i - z_j \rangle| + 2r \|V\| \\ &\leq M_2 \|z_i - z_j\| + 2rM_2 \\ &\leq M_2 \|x - x'\| + 2r(M_1 + M_2). \end{aligned}$$

This implies that  $\mathcal{V}_0 \subseteq \mathcal{V}$ , and the proof of Claim 1 is hence completed.  $\square$

Note that for any  $z \in \mathbb{R}^d$  and  $M > 0$ ,

$$\begin{aligned} \sigma^2 \operatorname{tr}(H(x)) &\leq \frac{\mathbb{E}_{X_0 \sim p_X} [\|X_0 - z\|^2 \exp(-\frac{\|x - X_0\|^2}{2\sigma^2})]}{\mathbb{E}_{X_0 \sim p_X} [\exp(-\frac{\|x - X_0\|^2}{2\sigma^2})]} \\ &\leq M^2 + \frac{\mathbb{E}_{X_0 \sim p_X} [(\|X_0 - z\|^2 - M^2)_+ \exp(-\frac{\|x - X_0\|^2}{2\sigma^2})]}{\mathbb{E}_{X_0 \sim p_X} [\exp(-\frac{\|x - X_0\|^2}{2\sigma^2})]}. \end{aligned}$$

Specialize the above to  $z = \bar{x} + V$  for  $\bar{x} \in \mathcal{X}_+$  and  $V \in \mathcal{V}$ , also fix  $M \geq 8(rM_1 + M_2)$ . Together, we have that

$$\begin{aligned}\sigma^2 \text{tr}(H(\bar{x} + V)) &\leq M^2 + \frac{\mathbb{E}_{X_0 \sim p_X}[(\|X_0 - \bar{x}\|^2 - M^2)_+ \exp(-\frac{\|\bar{x} + V - X_0\|^2}{2\sigma^2})]}{\mathbb{E}_{X_0 \sim p_X}[\exp(-\frac{\|\bar{x} + V - X_0\|^2}{2\sigma^2})]} \\ &= M^2 + \frac{\mathbb{E}_{X_0 \sim p_X}[(\|X_0 - \bar{x}\|^2 - M^2)_+ \exp(-\frac{\|\bar{x} - X_0\|^2 + 2\langle V, \bar{x} - X_0 \rangle}{2\sigma^2})]}{\mathbb{E}_{X_0 \sim p_X}[\exp(-\frac{\|\bar{x} - X_0\|^2 + 2\langle V, \bar{x} - X_0 \rangle}{2\sigma^2})]}.\end{aligned}$$

Using  $V \in \mathcal{V}$  and  $\bar{x}, x \in \bar{\mathcal{X}}$ , as long as  $\|\bar{x} - x\| \geq M$ , we know we can bound

$$|\langle V, \bar{x} - x \rangle| \leq M_2 \|\bar{x} - x\| + 2r(M_1 + M_2) \leq \frac{1}{4} \|\bar{x} - x\|^2,$$

and hence in this case  $\|\bar{x} - x\|^2 + 2\langle V, \bar{x} - x \rangle \geq \frac{1}{2} \|\bar{x} - x\|^2$ . This immediately implies that

$$\begin{aligned}&\mathbb{E}_{X_0 \sim p_X}[(\|X_0 - \bar{x}\|^2 - M^2)_+ \exp(-\frac{\|\bar{x} - X_0\|^2 + 2\langle V, \bar{x} - X_0 \rangle}{2\sigma^2})] \\ &\leq \mathbb{E}_{X_0 \sim p_X}[(\|X_0 - \bar{x}\|^2 - M^2)_+ \exp(-\frac{\|\bar{x} - X_0\|^2}{4\sigma^2})] \\ &\leq M^2 \exp(-\frac{M^2}{4\sigma^2}),\end{aligned}$$

where we use  $u \mapsto ue^{-u}$  is decreasing over  $u \geq 1$ .

On the other hand, suppose that  $\bar{x} \in B_i$  such that  $p_X(B_i) \geq \alpha$ . Note that for any  $x \in B_i$ , we can bound

$$\|\bar{x} - x\|^2 + 2\langle V, \bar{x} - x \rangle \leq 4r^2 + 4r \|V\| \leq 12\sigma^2 + 16\sigma^2 \sqrt{\log(2/\delta)}.$$

This implies that

$$\mathbb{E}_{X_0 \sim p_X}[\exp(-\frac{\|\bar{x} - X_0\|^2 + 2\langle V, \bar{x} - X_0 \rangle}{2\sigma^2})] \geq e^{-6-8\sqrt{\log(2/\delta)}} \mathbb{P}_{X_0 \sim p_X}(X_0 \in B_i) \geq c_0 \alpha \delta,$$

where  $c_0 > 0$  is an absolute constant.

Combining the above bounds, we can conclude that as long as  $\bar{x} \in \mathcal{X}_+$  and  $V \in \mathcal{V}$ ,  $M = 8(rM_1 + M_2) + 2\sigma \sqrt{\log(1/(c_0 \alpha \delta))}$ , it holds that

$$\sigma^2 \text{tr}(H) \leq M^2 + \frac{M^2}{c_0 \alpha \delta} \exp(-\frac{M^2}{4\sigma^2}) \leq 2M^2.$$

Note that  $\mathbb{P}_{\bar{x} \sim p_X}(\bar{x} \notin \mathcal{X}_+) \leq \sum_{i: p_X(B_i) < \alpha} p_X(B_i) \leq N\alpha = \delta$ , and hence

$$\mathbb{P}_{\tilde{\sigma}}(\sigma^2 \text{tr}(H(\bar{x} + V)) \leq 2M^2) \leq 2\delta.$$

Rescaling  $\delta \leftarrow \frac{\delta}{2}$  and plugging in the definition of  $M$  completes the proof of Eq. (29).

Similarly, we note that for  $V \in \mathcal{V}$ ,

$$\begin{aligned}\sigma^2 \cdot V^\top H(\bar{x} + V) V &\leq V^\top \mathbb{E}[(X_0 - \bar{x})(X_0 - \bar{x})^\top \mid X = \bar{x} + V] V \\ &= \mathbb{E}[\langle X_0 - \bar{x}, V \rangle^2 \mid X = \bar{x} + V] \\ &\leq \mathbb{E}[(M_2 \|X_0 - \bar{x}\| + 2r(M_1 + M_2))^2 \mid X = \bar{x} + V] \\ &\leq 2M_2^2 \mathbb{E}[\|X_0 - \bar{x}\|^2 \mid X = \bar{x} + V] + 8r^2(M_1 + M_2)^2.\end{aligned}$$

Our argument above then shows that

$$\mathbb{P}_{\tilde{\sigma}}(\sigma^2 \cdot V^\top H(\bar{x} + V)V \leq c_1 M^4) \leq 2\delta,$$

where  $c_1 > 0$  is an absolute constant. Rescaling  $\delta$  gives Eq. (30).

For the final claim, note that

$$\mathbb{E}[\|X - X_0\|^2 | X] = \|X - \bar{x}\|^2 - 2\langle X - \bar{x}, \mathbb{E}[X_0 - \bar{x} | X] \rangle + \mathbb{E}[\|X_0 - \bar{x}\|^2 | X].$$

Given  $X = \bar{x} + V$ ,

$$\begin{aligned} \mathbb{E}[\|X - X_0\|^2 | X] &= \|V\|^2 - 2\langle V, \mathbb{E}[X_0 - \bar{x} | X = \bar{x} + V] \rangle \\ &\quad + \mathbb{E}[\|X_0 - \bar{x}\|^2 | X = \bar{x} + V]. \end{aligned}$$

Using the claim above with the earlier bound on the third term implies

$$\begin{aligned} \mathbb{E}[\|X - X_0\|^2 | X] - \|V\|^2 &\lesssim M_2 \|\mathbb{E}[X_0 - \bar{x} | X = \bar{x} + V]\| \\ &\quad + r(M_1 + M_2) + \mathbb{E}[\|X_0 - \bar{x}\|^2 | X = \bar{x} + V] \\ &\lesssim M^2. \end{aligned}$$

Together with Gaussian concentration, the claim is complete.  $\square$

**Lemma F.4.** *It holds that*

$$\|W_\omega(X_t)\| \lesssim (R^2 \operatorname{tr}^2 C_\omega(X_t) + \operatorname{tr} C_\omega(X_t) Q_\omega(X, X_t))^{1/2}.$$

*Proof.* Cauchy–Schwarz gives

$$\|\operatorname{Cov}_{q_\omega}(X, \|Y - X\|^2 | Y = y)\| \leq \sqrt{\|C_\omega(y)\|_{\text{op}} \operatorname{Var}_{q_\omega}(\|Y - X\|^2 | Y = y)}.$$

For the first term,

$$\|C_\omega(y)\|_{\text{op}} \leq \operatorname{tr} C_\omega(y)$$

and for the second term

$$\begin{aligned} \operatorname{Var}_{q_\omega}(\|Y - X\|^2 | Y = y) &= \operatorname{Var}_{q_\omega}(-2\langle X, Y \rangle + \|X\|^2 | Y = y) \\ &\leq 8 \operatorname{Var}_{q_\omega}(\langle X, Y \rangle | Y = y) + 2 \operatorname{Var}_{q_\omega}(\|X\|^2 | Y = y) \\ &\lesssim \langle y, C_\omega(y) y \rangle + R^2 \operatorname{Var}_{q_\omega}(\|X\| | Y = y) \\ &\lesssim \langle X, C_\omega(y) X \rangle + \langle y - X, C_\omega(y) (y - X) \rangle \\ &\quad + R^2 \operatorname{Var}_{q_\omega}(\|X\| | Y = y) \\ &\lesssim R^2 \operatorname{tr} C_\omega(y) + Q_\omega(X, y). \end{aligned}$$

Plugging in  $X_t$  for  $y$  completes the proof.  $\square$

## G Experimental details

### G.1 Analytical blind denoiser

In this section we detail the of results shown in Section 4.1. Additionally, we present more examples of sampling from arbitrary mixture of high dimensional Gaussian embedded in low dimensions.

## Optimal denoiser for Gaussian Mixture

Take the true distribution to be a mixture of Gaussians with means  $m_i \in \mathbb{R}^d$  and fixed covariance matrix  $\Sigma_0 \succ 0$

$$p(x) = \frac{1}{K} \sum_{i=1}^K \mathcal{N}(x; m_i, \Sigma_0).$$

If we add centered Gaussian noise with variance  $\sigma^2$  to the data ( $x_\sigma = x + \sigma z$ ), the distribution of noisy images will be

$$p(x_\sigma) = \frac{1}{K} \sum_{i=1}^K \mathcal{N}(x; m_i, \Sigma_0 + \sigma^2 I).$$

Score of this density is

$$\nabla \log p(x_\sigma) = -(\Sigma_0 + \sigma^2 I)^{-1} \sum_{i=1}^K \omega_i(x_\sigma)(x_\sigma - m_i), \quad (33)$$

where

$$\omega_i(x_\sigma) = \frac{\mathcal{N}(x_\sigma; m_i, \Sigma_0 + \sigma^2 I)}{\sum_{j=1}^K \mathcal{N}(x_\sigma; m_j, \Sigma_0 + \sigma^2 I)}.$$

So the optimal denoiser for a noisy observation can be written in closed-form as

$$f^*(x_\sigma, \sigma, \{m_i\}_{i=1}^K, \Sigma_0) = x_\sigma - \sigma^2 I (\Sigma_0 + \sigma^2 I)^{-1} \sum_{i=1}^K \omega_i(x_\sigma)(x_\sigma - m_i). \quad (34)$$

To sample with the blind denoiser, we estimate the noise variance from a single noisy data point by maximizing the likelihood of noisy observation across  $\log p_\sigma$ . Thus, for a given noisy observation  $y$ , we compute  $\hat{\sigma}$  such that

$$\hat{\sigma} = \operatorname{argmax}_\sigma \log p_\sigma(y)$$

The *blind* denoiser under maximum likelihood estimation (MLE) of the noise variance is therefore

$$f^\dagger(x_\sigma, \hat{\sigma}, \{m_i\}_{i=1}^K, \Sigma_0) = x_\sigma - \hat{\sigma}^2 I (\Sigma_0 + \hat{\sigma}^2 I)^{-1} \sum_{i=1}^K \omega_i(x_\sigma)(x_\sigma - m_i). \quad (35)$$

---

**Algorithm 3** Sampling using an optimal blind denoiser with MLE noise variance

---

**Input:** Optimal denoiser  $f^\dagger$ , stepsize  $h > 0$ , diffusion coefficients  $(a_t)_{t \in [0, T]}$ , model parameters  $\{m_i\}_{i=1}^K, \Sigma_0$ , and  $\sigma_0, \sigma_T > 0$

**Initialize**  $X_0 \sim \mathcal{N}(0, \sigma_0^2 I)$ ,  $k = 0$

**while**  $\text{keepgoing} == \text{True}$  **do**

    Compute  $\hat{\sigma}_k = \text{argmax}_\sigma \log p_\sigma(X_{kh})$

$s_k = f^\dagger(X_{kh}, \hat{\sigma}, \{m_i\}_{i=1}^K, \Sigma_0) - X_{kh}$

**if**  $\hat{\sigma}_k \leq \sigma_T$  **then**

$\text{keepgoing} \leftarrow \text{False}$

**else**

        Update  $X_{(k+1)h} \leftarrow X_{kh} + hs_k + \sqrt{2} \int_{kh}^{(k+1)h} a_t dB_t$

**end if**

**end while**

---

### More examples

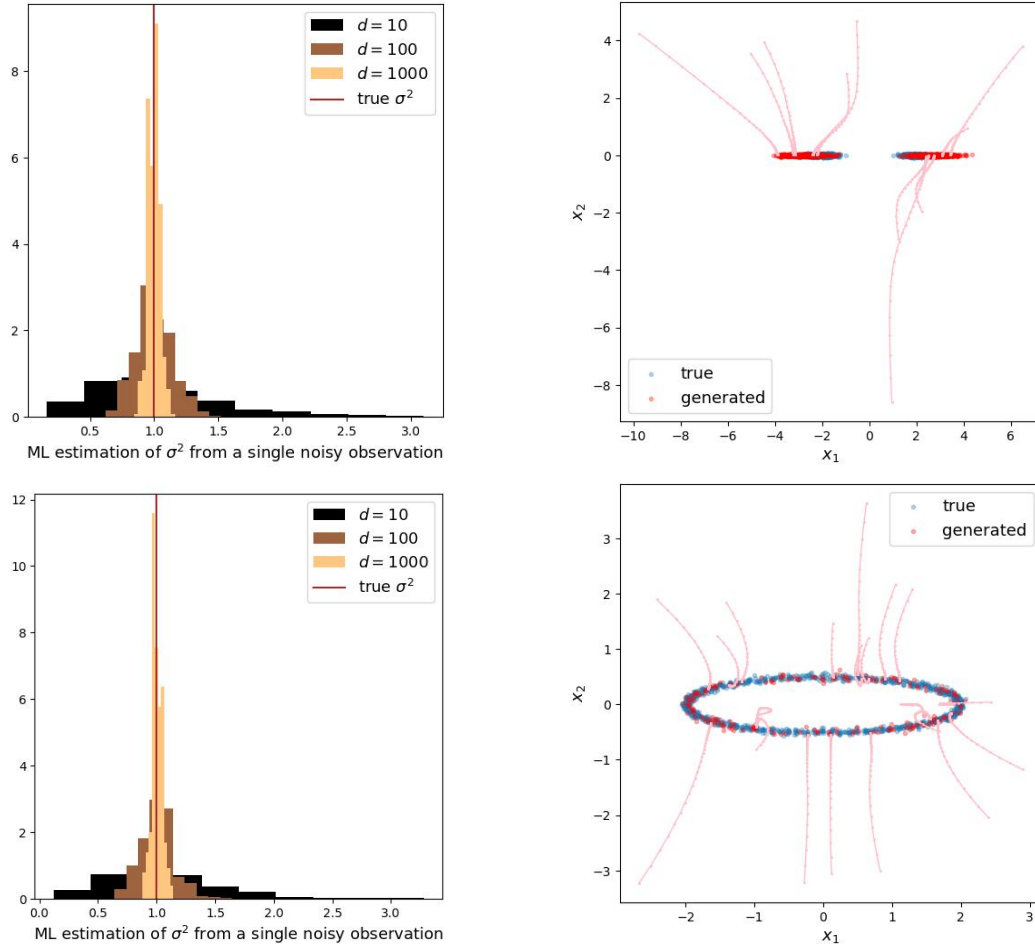


Figure 10: **Top:** Mixture of two Gaussians with covariances of rank  $k = 1$ . On the left, the effect of increasing ambient dimensionality,  $d$  is shown. On the right, sampling is shown for  $d = 1000$ . **Bottom:** Ellipse constructed as a mixture of Gaussians. Sampling is shown for  $d = 100$ .

## G.2 Blind denoisers trained on Gaussian and Gaussian mixture data

We present two sets of experiments on toy data that elucidate the impact of intrinsic dimensionality and blind denoising. In both cases, we use a 6-layer MLP with width 512 and ReLU activations. We use the default AdamW optimizer in PyTorch, with learning rate equal to  $10^{-3}$ , and train for 50k steps with batch size equal to 512. We take  $\sigma_T = 0.01$  and  $\sigma_0 = 10$ . Additionally,  $\Theta$  was chosen to be a log-uniform prior on  $[\sigma_T, \sigma_0]$ .

### Gaussian data

We randomly generate a  $k \times k$  covariance  $\Sigma$  matrix, with  $k = 2$ . We generate  $n = 5000$  points from  $\mathcal{N}(0, \Sigma)$  and train two blind denoisers, denoted  $\hat{f}_\theta^{(2)}$  and  $\hat{f}_\theta^{(100)}$ . In the first scenario, the input dimension is the same as the intrinsic dimension of the data. In the latter, we pad the data with zeros until the data dimension is  $d = 100$ , thus changing the input dimension of the network.

Figure 3 displays the output from Algorithm 2 using an exponential Euler integrator with  $h = 0.5$  and  $a_t = 0.5\sigma_t^2$ . We see that the generated samples for  $k = d = 2$  are heavily concentrated and do not accurately capture the training data. Moreover, the noise schedule is both too fast at the beginning and too slow at inference. In contrast, the blind denoiser trained with larger input dimension manages to both (i) generate viable samples, and (ii) obey the noise schedule from Proposition 3.2 exactly.

### Gaussian-mixture data

We repeat the same experiment on 2-component Gaussian mixture data using randomly generated means and covariances with equal weight with  $k = 2$ . We use  $n = 50000$  datapoints and additionally incorporated weight-decay in the AdamW optimizer of value  $5 \times 10^{-2}$ . All other parameters remain the same, except now  $d \in \{2, 200\}$ . The behavior is essentially identitcal to Figure 3, where low intrinsic and high ambient dimensionalities are crucial for blind denoisers to learn and sample from the data distribution.

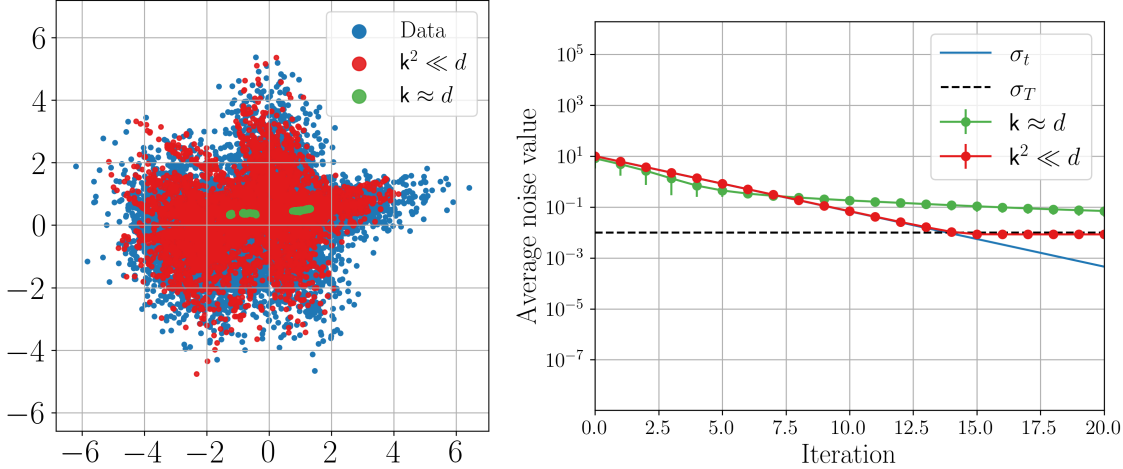


Figure 11: Sampling performance of BDDMs trained on a mixture of Gaussian dataset with intrinsic dimension  $k = 2$  and two different input dimensions  $d \in \{2, 200\}$ . Generated samples (left) and evolution of the estimated noise level, corresponding to Proposition 3.2 (right).

### G.3 Photographic images

#### Architecture

The U-Net is the most widely used architecture for denoising and score estimation. We adopt the vanilla U-Net (Ronneberger et al., 2015), composed of convolutional layers with ReLU nonlinearities and layer normalization, organized into downsampling and upsampling blocks. In more detail, there are 3 downsampling and 3 upsampling blocks with increasing number of channels [64, 128, 256]. The middle block has 512 channels. There are also 3 skip connections that carry details from each encoder to the corresponding decoder at the same scale. The number of layers in the encoding blocks is 2 and decoding blocks is 6.

For non-blind models, we use the standard noise-level embedding: the noise level is mapped through a Fourier feature transform, processed by an MLP, and injected into all normalization layers via scale and shift parameters.

Our goal is to match architectural and training hyperparameters as closely as possible (except for noise conditioning versus blindness) to enable fair comparisons, so all models are trained from scratch. The architecture is intentionally small (**around 13 million parameters**) and simple (e.g., no attention or text conditioning) compared to commonly used models with hundreds of millions of parameters; the goal is not SOTA performance but a controlled comparison of blind versus non-blind models.

#### Training

Blind models are trained by minimizing the empirical loss in (6), following Algorithm 1, while non-blind models are trained using the noise-conditioned counterpart. The noise level  $\sigma \in (0, 3]$  is sampled according to  $1/\sqrt{\sigma}$ . We use a batch size of 512 for all models. The learning rate is 0.001 with a rate of decay of 100. We fix the total number of epochs (i.e. full pass one the dataset) to 1000. Training is done on 4 GPU H100 NVIDIA GPUs per model, taking around 24 hours for CelebA and 34 hours for Bedroom datasets.

We observe diminishing mean-square error improvements as increases when the model is trained to predict the clean image; this generalization beyond the training noise range does not hold for models trained to predict the residual directly. This suggests that neural networks more readily represent constants (e.g., zero or the data mean) than the identity mapping.

### Noise level estimator model

We train a small network to estimate the noise level from a given noisy image. Given the simplicity of this task, our network consists of 4 convolutional layers with filter size of  $3 \times 3$ , and the number of channels in the intermediate layers is 64. To match the denoisers, we choose  $\sigma \in (0, 3]$ . The trained model can estimate the noise level almost perfectly, as seen in Figure 12.

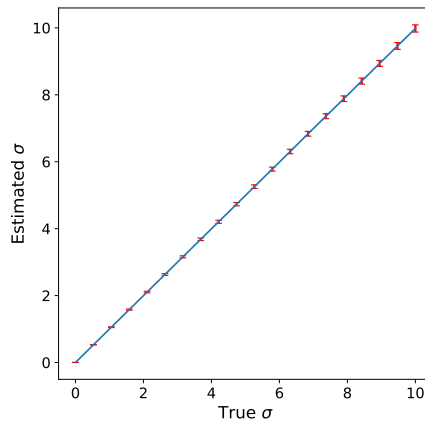


Figure 12: A smaller neural network trained to estimate  $\sigma$  from noisy image is very accurate. Error bars show two standard deviation. It is also worth noting that the model performs well beyond training range  $\sigma \in (0, 3]$ .